

Peculiar architectures for the WASP-53 and WASP-81 planet-hosting systems^{*}

Amaury H. M. J. Triaud^{1,2,3,4†}, Marion Neveu-VanMalle^{1,5}, Monika Lendl^{6,1}, David R. Anderson⁷, Andrew Collier Cameron⁸, Laetitia Delrez⁹, Amanda Doyle¹⁰, Michaël Gillon⁹, Coel Hellier⁷, Emmanüel Jehin⁹, Pierre F. L. Maxted⁷, Damien Ségransan¹, Barry Smalley⁷, Didier Queloz^{5,1}, Don Pollacco¹⁰, John Southworth⁷, Jeremy Tregloan-Reed^{11,7}, Stéphane Udry¹, Richard West¹⁰

¹ *Observatoire Astronomique de l'Université de Genève, Chemin des Maillettes 51, CH-1290 Sauverny, Switzerland*

² *Institute of Astronomy, University of Cambridge, Madingley Road, CB3 0HA, Cambridge, United Kingdom*

³ *Centre for Planetary Sciences, University of Toronto at Scarborough, 1265 Military Trail, Toronto, ON, M1C 1A4, Canada*

⁴ *Department of Astronomy & Astrophysics, University of Toronto, Toronto, ON, M5S 3H4, Canada*

⁵ *Cavendish Laboratory, J J Thomson Avenue, Cambridge CB3 0HE, UK*

⁶ *Space Research Institute, Austrian Academy of Sciences, Schmiedlstr. 6, 8042 Graz, Austria*

⁷ *Astrophysics Group, Keele University, Staffordshire, ST5 5BG, UK*

⁸ *SUPA, School of Physics & Astronomy, University of St. Andrews, North Haugh, KY16 9SS, St. Andrews, Fife, Scotland, UK*

⁹ *Institut d'Astrophysique et de Géophysique, Université de Liège, Allée du 6 Août 17, Sart Tilman, 4000 Liège 1, Belgium*

¹⁰ *Department of Physics, University of Warwick, Coventry CV4 7AL, UK*

¹¹ *SETI Institute, Mountain View, CA, 94043, USA*

Accepted ?. Received ?; in original form ?

ABSTRACT

We report the detection of two new systems containing transiting planets. Both were identified by WASP as worthy transiting planet candidates. Radial-velocity observations quickly verified that the photometric signals were indeed produced by two transiting hot Jupiters. Our observations also show the presence of additional Doppler signals. In addition to short-period hot Jupiters, we find that the WASP-53 and WASP-81 systems also host brown dwarfs, on fairly eccentric orbits with semi-major axes of a few astronomical units. WASP-53c is over $16 M_{\text{Jup}} \sin i_c$ and WASP-81c is $57 M_{\text{Jup}} \sin i_c$. The presence of these tight, massive companions restricts theories of how the inner planets were assembled. We propose two alternative interpretations: a formation of the hot Jupiters within the snow line, or the late dynamical arrival of the brown dwarfs after disc-dispersal.

We also attempted to measure the Rossiter–McLaughlin effect for both hot Jupiters. In the case of WASP-81b we fail to detect a signal. For WASP-53b we find that the planet is aligned with respect to the stellar spin axis. In addition we explore the prospect of transit timing variations, and of using *Gaia*'s astrometry to measure the true masses of both brown dwarfs and also their relative inclination with respect to the inner transiting hot Jupiters.

Key words: planetary systems – planets and satellites: individual: WASP-81, WASP-53 – binaries: eclipsing – brown dwarfs

1 FOREWORDS

The discovery of 51 Peg b (Mayor & Queloz 1995) initiated a debate about the origin (formation and evolution) of

^{*} using data collected at ESO's La Silla Observatory, Chile: HARPS on the ESO 3.6m (Prog IDs 087.C-0649, 089.C-0151, 090.C-0540, 091.C-0184 & 093.C-0474), the ESO NTT (Prog ID 088.C-0204), the Swiss *Euler* telescope, and TRAPPIST. The data is publicly available at the *CDS* Strasbourg and on demand to the main author.

† E-mail: aht34@cam.ac.uk

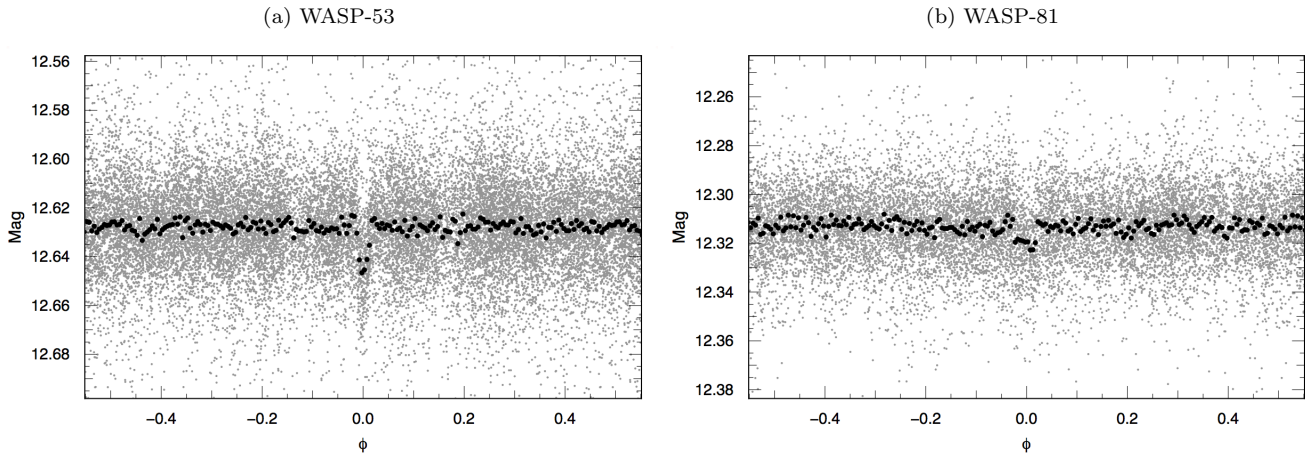


Figure 1. Variations in the magnitude of WASP-53 and WASP-81 leading to their identification as transiting planet candidates. The grey dots show individual WASP measurements, whereas the black dots show the median magnitude within each of 200 phase bins.

hot Jupiters that continues to rage to this day. The question is whether they formed in situ, within the so-called *snow line* (Bodenheimer, Hubickyj & Lissauer 2000; Batygin, Bodenheimer & Laughlin 2015; Lee & Chiang 2015), or beyond, followed by inward migration (Pollack et al. 1996; Alibert et al. 2005; Helled et al. 2014). The second hypothesis needs an explanation of how hot Jupiters have migrated, either via angular momentum transfer with their protoplanetary disc (Lin, Bodenheimer & Richardson 1996; Ward 1997; Baruteau et al. 2014) or thanks to dynamical interactions followed by tidal circularisation (high-eccentricity migration) (Rasio & Ford 1996; Wu, Murray & Ramsahai 2007; Naoz et al. 2011; Petrovich 2015a). Any framework has to explain why gas giants are found both close and far from their host star (not least Jupiter and Saturn), and also that they frequently orbit on planes that are inclined, sometimes retrograde, with respect to the equatorial plane of their host star (Hébrard et al. 2008; Winn et al. 2009; Schlaufman 2010; Anderson et al. 2010; Triaud et al. 2010; Albrecht et al. 2012a; Lendl et al. 2014; Winn & Fabrycky 2015).

Observations of the spin-orbit angle, thanks to the Rossiter–McLaughlin effect (Queloz et al. 2000), were initially thought to provide a clean test between disc-driven migration and dynamical and tidal migration (Gaudi & Winn 2007). While some studies indicate that observations are compatible with planets undergoing orbital realignment (Triaud 2011; Albrecht et al. 2012b; Dawson 2014), additional theoretical arguments imply that misalignments can arise via a variety of processes. They can be primordial, with the planets forming on inclined planes (Thies et al. 2011; Lai, Foucart & Lin 2011; Batygin 2012; Lai 2014; Spalding & Batygin 2015), or they can arise later (Cébron et al. 2011; Rogers et al. 2013). Thus inclined hot Jupiters are compatible with both dynamical interactions and with disc-driven migration.

Obviously, disc-driven migration and high-eccentricity migration could both be correct and each produce a fraction of the hot Jupiters, as recent observation appear to imply (Anderson et al. 2015). Finally, results from Guillochon, Ramirez-Ruiz & Lin (2011) suggest that high-eccentricity

migration requires in most cases some amount of disc-driven migration.

In this paper, we spend the first sections to describe the discovery of two new planetary systems. Both present a tight hierarchical architecture, composed of an inner, transiting, hot Jupiter, and an outer brown-dwarf companion. WASP-53 & WASP-81 are reminiscent of a challenge proposed by Hatzes & Wuchterl (2005) to test disc-driven migration. If both brown dwarfs were on their current orbits during the protoplanetary phase, they would have truncated the disc within the *snow line* thus preventing disc-driven migration and only allowing *in-situ* formation.

In the final sections we describe a number of formation and evolution scenarios, some involving disc-driven migration and others not. We conclude that a number of scenarios will become testable soon, with the arrival of precise astrometric measurements produced by ESA’s *Gaia* satellite. We also compute the equilibrium eccentricities of the inner gas giants (Mardling 2007) and find it is unlikely that their k_2 Love number (Batygin, Bodenheimer & Laughlin 2009) will be measured soon.

2 WASP IDENTIFICATION

The WASP survey¹ (Pollacco et al. 2006) consists of two sets of eight 11-cm refractive telescope mounted together. One set is located at the Observatorio del Roque de Los Muchachos, La Palma (Spain), while the other is installed in Sutherland, hosted by the South African Astronomical Observatory. WASP has observed in excess of 30 million stars since 2004, thousands of times each. The photometric data reduction and the candidate selection are described in Collier Cameron et al. (2007).

WASP-53 (2MASS J02073820–2039426; K3, $J = 10.959$) and WASP-81 (2MASS J20164989+0317385; F9, $J = 11.263$) have been observed 21 120 and 13 292 times by WASP. They were two unremarkable and anonymous stars before a short, box-like photometric signals were identified at $P = 3.309866$ d and $P = 2.716554$ d, respectively.

¹ <https://wasp-planets.net>

WASP-53b was sent for radial-velocity verification in 2010-08-10, and WASP-81b in 2011-05-09, with the first spectra acquired on 2010-12-05 and 2011-09-29. The WASP data are shown in Fig. 1.

3 PHOTOMETRIC OBSERVATIONS

All follow-up photometric timeseries, their dates, filters, number of data points and the detrending functions that were used in the analysis, are detailed in Table C1. Figure 3 shows the corrected photometry for WASP-53, and Figure 4 shows WASP-81. Raw fluxes and residuals are shown in Figure C1 & C2, respectively. Below, we provide some details on the observations and reduction, although we encourage readers to refer to cited papers for fuller information.

3.1 EulerCam

EulerCam is mounted at the 1.2m *Euler* Swiss telescope located at ESO La Silla Observatory (Chile) It has a pixel scale of $0.215''$ for a field of view of $14.7 \times 14.5'$. The telescope is an alt-azimuthal design. EulerCam is mounted behind a field de-rotator. To ensure the best photometric precision, each star is kept on the same pixels, using a digital feedback scheme that compares the newly acquired frame with a composite of earlier frames and their offset from a recorded position.

We obtained four transits of WASP-53b, all using an r' -Gunn filter, and with a slightly defocused telescope to improve the observing efficiency and PSF sampling. Two of the transit, on 2011-09-22 and 2012-12-02 were scheduled to coincide with the radial-velocity time-series obtained using HARPS (see Sect 4.2). WASP-81 was observed with EulerCam throughout three transits, one of which, on 2013-08-05, was obtained while HARPS collected a radial-velocity time-series. Our 2012-06-07 observations were obtained using an I -Cousins filter, and a focused telescope. The telescope was defocused slightly for latter two observations, for which a z' -Gunn (2012-09-24) and an r' -Gunn (2013-08-05) were used.

All EulerCam images were reduced using standard image correction methods and lightcurves were obtained using differential aperture photometry, with a careful selection of aperture and reference stars. For further details on the EulerCam instrument and the associated data reduction procedures, please refer to Lendl et al. (2012). The times of observations are provided in JD(UTC), changed later to BJD(TDB) during the global analysis.

3.1.1 A nearby stellar source

During spectroscopic observations an additional light source was noticed near WASP-81A on CORALIE's guiding camera images. On 2014-04-29 we obtained focused images of the WASP-81 system with EulerCam through Geneva B (6 images), Geneva V (3 images) and r' -Gunn (3 images) filters (Fig. 2). We used astronomy.net (Lang et al. 2010) to calculate a precise astrometric solution and performed PSF fitting on the images using DAOPHOT (Stetson 1987). The results are in Table 1.

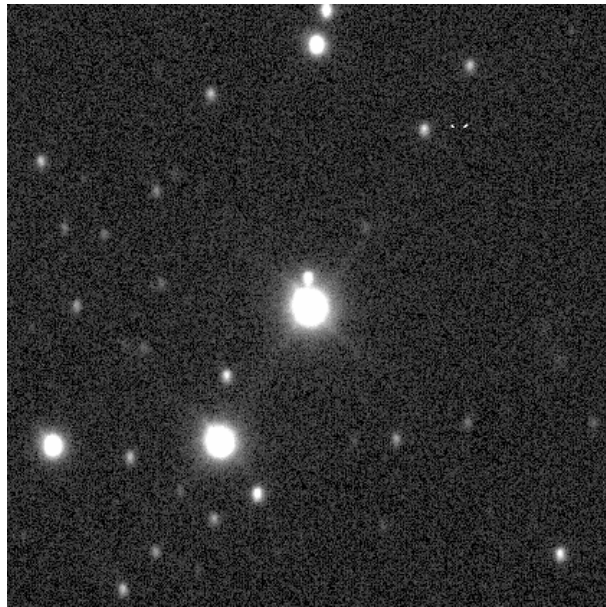


Figure 2. A $1.5' \times 1.5'$ field of view centred on WASP-81, obtained with EulerCam, clearly showing a visual companion to the North. The pair is most likely unrelated.

Table 1. Observation parameters for the companion source to WASP-81A

Filter	Δ Mag	Mag	separation (arcsec)	PA (degrees)
BG	5.64 ± 0.03	18.78 ± 0.07	4.34 ± 0.02	3.5 ± 0.2
VG	5.16 ± 0.01	17.61 ± 0.02	4.33 ± 0.01	3.5 ± 0.3
r'	4.87 ± 0.01	17.14 ± 0.04	4.32 ± 0.01	3.5 ± 0.3
<i>weighted mean:</i>			4.33 ± 0.01	3.5 ± 0.3

We extracted magnitudes for the visual companion relative to the primary target. Combining with apparent magnitudes for WASP-81A (Table 2), and using a $E(B - V) = 0.05$ (Sect. 4), we obtained apparent magnitudes for the visual companion. We find that the companion has colours consistent with a K3–K4 spectral type. If it is a dwarf, this implies a distance modulus of order 10.2 (1.1 kpc), compared to 8.0 (400 pc) for WASP-81A; if it were a giant it would be further away still. If we place the companion on a main-sequence isochrone (Marigo et al. 2008), and if WASP-81A were at the same distance, WASP-81A would have to be a 2-Gyr old, $1.4\text{--}1.6 M_{\odot}$ star, contradicting our spectroscopic analysis as well as the mean stellar density obtained from the transit. If, instead, WASP-81A is on the main sequence, then the companion has to be below the main sequence to be at the same distance. The two objects are most therefore likely unrelated. We placed an HR diagram of the pair into the appendices.

For future reference we provide here the position of the visual companion. *Gaia* will soon produce parallaxes and proper motions that should confirm our analysis. If instead they are found at the same distance, implying they are gravitationally bound, then the companion must be an M dwarf with a much redder $B - V$ than the one we measured.

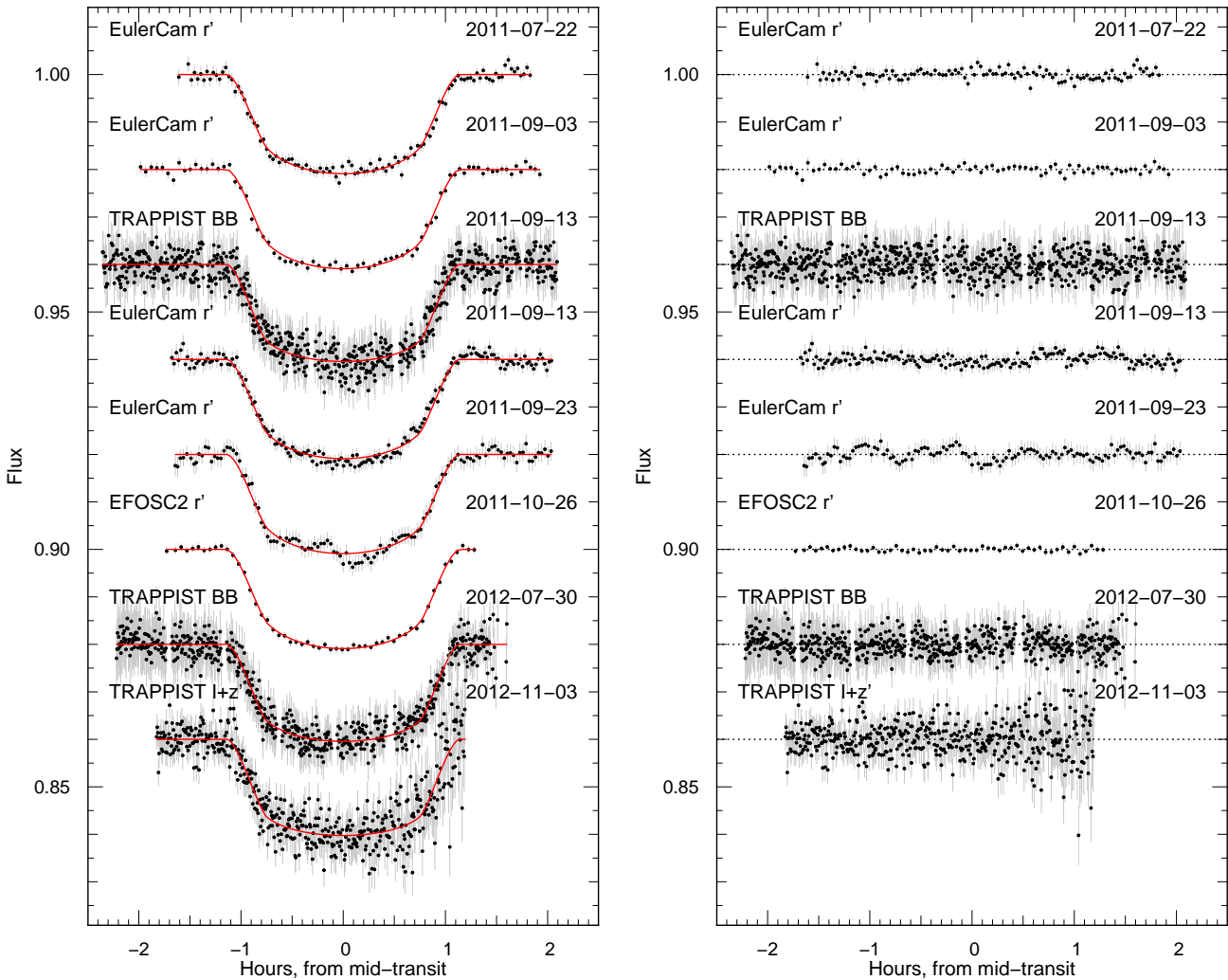


Figure 3. Photometry on WASP-53 at the time of transit, using EulerCam, TRAPPIST and the NTT. *Left*, we have the detrended data with, in red, the most likely model. *Right*, we show the residuals. Raw photometry and full models are available in Fig. C1.

3.2 TRAPPIST

Both WASP systems were observed with the 0.6-m TRAPPIST robotic telescope (TRAnSiting Planets and Planetes-Imals Small Telescope), also located at La Silla. Three transits were obtained on WASP-53, and seven on WASP-81. TRAPPIST is equipped with a thermoelectrically-cooled $2K \times 2K$ CCD, which has a pixel scale of $0.6''$ that translates into a $22' \times 22'$ field of view. For details of TRAPPIST, see Gillon et al. (2011) and Jehin et al. (2011). Two filters were used: a blue-blocking filter that has a transmittance of $> 90\%$ from 500 nm to beyond 1000 nm, and an “ $I + z'$ ” filter that has a transmittance of $> 90\%$ from 750 nm to beyond 1100 nm. During the runs the positions of the stars on the chip were maintained to within a few pixels thanks to a “software guiding” system that regularly derives an astrometric solution for the most recently acquired image and sends pointing corrections to the mount if needed. After a standard pre-reduction (bias, dark, and flatfield correction), the stellar fluxes were extracted from the images using

the IRAF/DAOPHOT² aperture photometry software (Stetson 1987). For each light curve we tested several sets of reduction parameters and kept the one giving the most precise photometry for the stars of similar brightness as the target. After a careful selection of reference stars the transit light curves were finally obtained using differential photometry. Some light curves were affected by a meridian flip; that is, the 180° rotation that the German equatorial mount telescope has to undergo when the meridian is reached. This movement results in different positions of the stellar images on the detector before and after the flip, and thus in a possible jump of the differential photometry at the time of the flip. We have accounted for this in our light curve analysis by including a normalization offset in our model at the time of the flip (see Fig. C1 & C2 as well as Table C1). More details on data acquisition and data reduction can be found

² IRAF is distributed by the National Optical Astronomy Observatory, which is operated by the Association of Universities for Research in Astronomy, Inc., under cooperative agreement with the National Science Foundation.

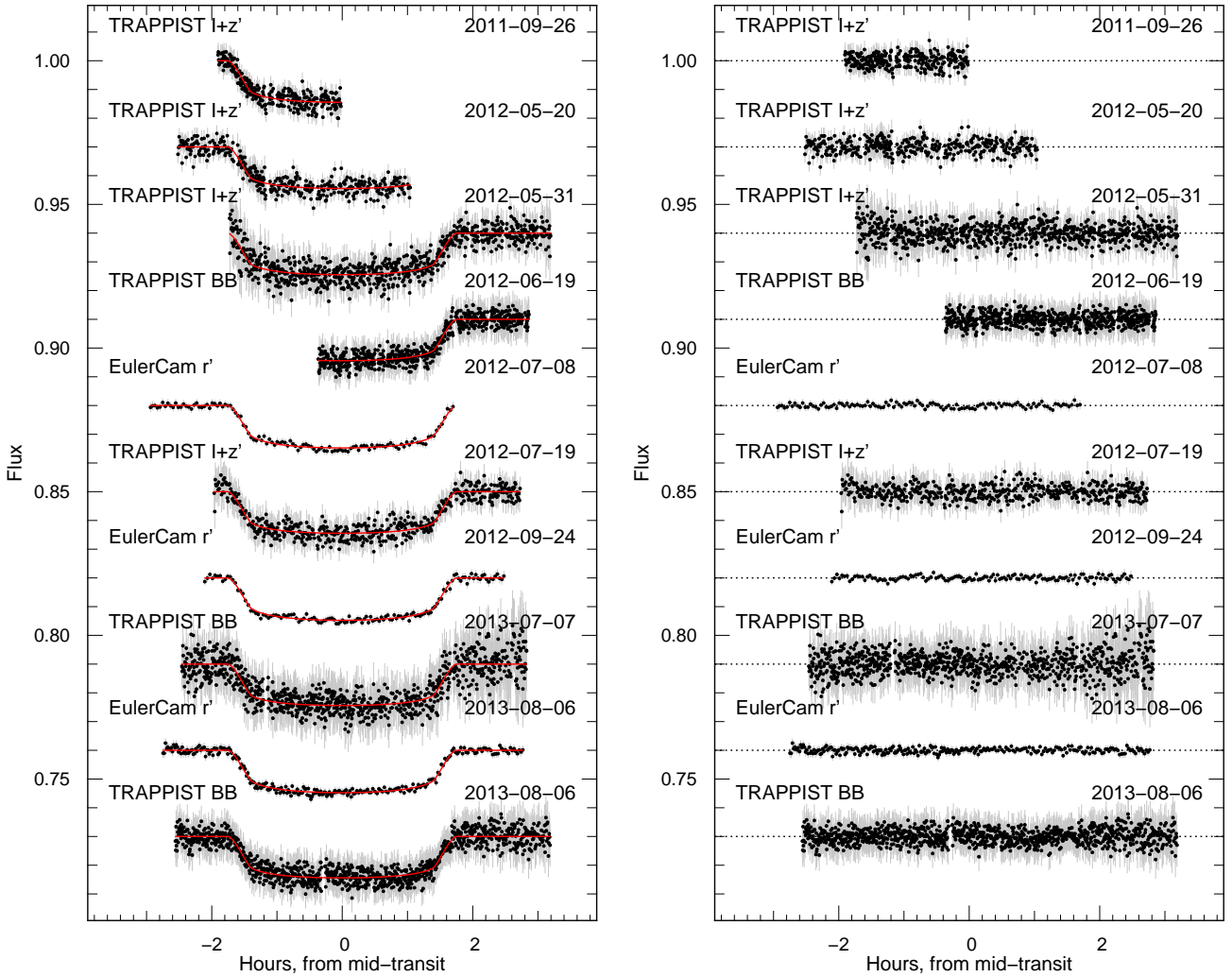


Figure 4. Photometry on WASP-81 at the time of transit, using EulerCam and TRAPPIST. *Left*, we show the detrended data with, in red, the most likely model. *Right*, we show the residuals. Raw photometry and full models are available in Fig. C2.

in Gillon et al. (2013) and Delrez et al. (2014), whose procedures were followed here as well. The times of observations are provided in JD(UTC), changed later to BJD(TDB) during the global analysis.

3.3 New Technology Telescope

One transit of WASP-53 was observed using the EFOSC2 instrument on the NTT at ESO’s observation of La Silla (ProgID 088.C-0204, PI Tregloan-Reed; see Tregloan-Reed & Southworth (2013) for further details of this observing run). The instrument has a $2K \times 2K$ CCD covering a $4.1' \times 4.1'$ field of view, and a pixel scale of $0.12''$. Observations were curtailed shortly after the end of the transit due to the onset of daytime. We observed through a Gunn r filter (ESO filter #784) with heavy defocussing and exposure times of 150s.

The data were reduced using the DEFOT pipeline (Southworth et al. 2009), which utilises an aperture-photometry routine APER.PRO ported from DAOPHOT (Stetson 1987). The radius of the inner aperture was 45 pixels

and the sky annulus extended from 60 to 100 pixels. Debiassing and flat-fielding the data did not make a significant difference to the results, so we neglected these calibrations.

A differential-photometry light curve was obtained for WASP-53 versus an ensemble comparison star. Due to the small field of view of NTT/EFOSC2, we were able to use only three comparison stars, all of which were at least two magnitudes fainter than WASP-53 in the r -band. The weights of the comparison stars, used in summing their fluxes to create the ensemble comparison star, were optimised to minimise the scatter in the data outside transit. Finally, the timestamps were moved to the BJD(TDB) timescale using routines from Eastman, Siverd & Gaudi (2010).

4 SPECTROSCOPIC OBSERVATIONS

We collected 98 CORALIE spectra on WASP-53 between the dates of 2010-12-04 and 2016-11-21, as well as 83 HARPS spectra between the date of 2011-08-28 and 2014-09-28. On WASP-81, we acquired 67 spectra with

CORALIE from 2011-09-28 to 2015-07-08, and 32 using HARPS between 2013-04-20 and 2016-10-21.

4.1 Spectral analysis

The analysis was performed on the standard pipeline reduction products, using the methods given in [Doyle et al. \(2013\)](#). The H_α line was used to give an initial estimate of the effective temperature (T_{eff}). The surface gravity ($\log g_\star$) was determined from the Ca I line at 6439Å, along with the Na I D lines. Additional T_{eff} and $\log g_\star$ diagnostics were performed using the Fe lines. An ionisation balance between Fe I and Fe II was required, along with a null dependence of the abundance on either equivalent width or excitation potential. This null dependence was also required to determine the microturbulence (ξ_t). The parameters obtained from the analysis are listed in [Table 2](#). Some of those parameters will later be employed as priors to compute the most likely physical parameters of each system. The elemental abundances were determined from equivalent width measurements of several clean and unblended lines, and additional least squares fitting of lines was performed when required. The quoted error estimates include that given by the uncertainties in T_{eff} , $\log g_\star$, and ξ_t , as well as the scatter due to measurement and atomic data uncertainties.

The individual HARPS spectra of WASP-53 were co-added to produce a single spectrum with an average S/N in excess of 100:1. The macroturbulence was assumed to be zero, since for mid-K stars it is expected to be lower than that of thermal broadening ([Gray 2008](#)). The projected stellar rotation velocity ($v \sin i_\star$) was determined by fitting the profiles of several unblended lines, yielding an upper limit of $2.7 \pm 0.3 \text{ km s}^{-1}$ for WASP-53. There is no significant detection of lithium in WASP-53. The equivalent width upper limit of 13mÅ, correspond to an abundance upper limit of $\log A(\text{Li}) < 0.32 \pm 0.16$. This implies an age of at least several hundreds Myr ([Sestito & Randich 2005](#)).

Similarly, the combination of the HARPS spectra obtained on WASP-81 produced a combined spectrum with an average S/N of 60:1. Here, we used a macroturbulent value of $3.84 \pm 0.73 \text{ km s}^{-1}$ after a relation from [Doyle et al. \(2014\)](#). $v \sin i_\star$ was found to be $1.20 \pm 0.69 \text{ km s}^{-1}$.

4.2 Radial velocities

The spectra were reduced using the standard CORALIE and HARPS reduction software. They have been shown to reach remarkable precision and accuracy, reaching below 1 m s^{-1} (e.g. [Lovis et al. \(2006\)](#); [Marmier et al. \(2013\)](#); [López-Morales et al. \(2014\)](#)). We extracted the radial velocities for both stars by cross-correlating each spectrum with a binary mask. For WASP-53A we used a mask corresponding to a K5 spectral type, and for WASP-81A we employed a G2 mask. We fit the corresponding cross-correlation function with a Gaussian, whose mean provides us with the radial velocity ([Baranne et al. 1996](#)). The corresponding values are displayed in the Journal of Observations ([Appendix B](#)), along with observational data such as the individual exposure times. The observations are graphically presented in [Fig. 5a](#) for WASP-53 and in [Fig. 5b](#) for WASP-81.

Table 2. Stellar parameters of WASP-53A and WASP-81A

Parameter	WASP-53A	WASP-81A
α	02 ^h 07'38.22''	20 ^h 16'49.89''
δ	-20°39'43.0''	+03°17'38.7''
m_B	17.46 ± 0.30 ^a	13.14 ± 0.30 ^a
m_V	12.19 ± 0.30 ^b	12.29 ± 0.10 ^b
m_R	11.85 ± 0.30 ^a	12.67 ± 0.30 ^a
$m_{r'}$	12.29 ± 0.30 ^c	12.36 ± 0.30 ^c
m_I	11.653 ± 0.020 ^d	11.326 ± 0.053 ^b
m_J	10.959 ± 0.026 ^e	11.263 ± 0.027 ^e
m_H	10.474 ± 0.022 ^e	10.913 ± 0.024 ^e
m_K	10.390 ± 0.023 ^e	10.892 ± 0.026 ^e
T_{eff} (K)	4950 ± 60	5890 ± 120
$\log g_\star$ (km s^{-1})	4.40 ± 0.20	4.27 ± 0.09
ξ_t (km s^{-1})	0.60 ± 0.25	0.94 ± 0.15
$v \sin i_\star$ (km s^{-1})	< 2.7 ± 0.3	1.20 ± 0.73
[Fe/H]	0.22 ± 0.11	-0.36 ± 0.14
[Ca/H]	0.16 ± 0.15	-0.25 ± 0.09
[Sc/H]	0.19 ± 0.11	-0.18 ± 0.18
[Ti/H]	0.26 ± 0.15	-0.14 ± 0.11
[V/H]	0.44 ± 0.20	-0.29 ± 0.12
[Cr/H]	0.22 ± 0.11	-0.40 ± 0.11
[Mn/H]	0.29 ± 0.20	-0.55 ± 0.09
[Co/H]	0.24 ± 0.11	-0.36 ± 0.14
[Ni/H]	0.20 ± 0.12	-0.34 ± 0.15
$\log A(\text{Li})$	< 0.32 ± 0.16	1.21 ± 0.10
Mass (M_\odot)	0.87 ± 0.08	1.04 ± 0.09
Radius (R_\odot)	0.96 ± 0.24	1.24 ± 0.15
Spectral Type	K3	G1
Distance (pc)	235 ± 55	410 ± 70

Note: Mass and Radius estimate using the [Torres, Andersen & Giménez \(2010\)](#) calibration. Spectral Type estimated from T_{eff} using the table in [Gray \(2008\)](#). Abundances are relative to the solar values obtained by [Asplund et al. \(2009\)](#). references a) NOMAD; ([Zacharias et al. 2004](#)) b) TASS; ([Droege et al. 2006](#)) c) CMC14; ViZier I/304/out d) DENIS; ([DENIS Consortium 2005](#)) e) 2MASS; [Skrutskie et al. \(2006\)](#)

4.2.1 WASP-53

We first started to monitor WASP-53A with CORALIE, on 2010-12-05 targeting the orbital phase 0.75. The second spectrum was obtained 28 nights later, close to phase 0.25, and revealed a blue-shifted movement of nearly 400 m s^{-1} , compatible with a planetary object. The star was immediately flagged for intense follow-up, with the third spectrum acquired two nights after the second. The star was moving rapidly, and there was no sign of a change in the line width (FWHM), nor of its shape (span of the bisector slope), as can be visually inspected in [Figs. 5](#) and [6](#). However, despite being obtained at phase 0.81, the star's velocity was puzzling, being red-shifted by 300 m s^{-1} compared to the first epoch. Our strategy has always been to follow any radial-velocity movement and identify its origin, planetary or not. Observations were continued.

Before the observing season was over, we had confirmed a radial-velocity oscillation at a period matching the WASP signal (caused by WASP-53b), plus a rapid rise in the radial velocity. The following season we observed with both HARPS and CORALIE. WASP-53b's motion was quickly

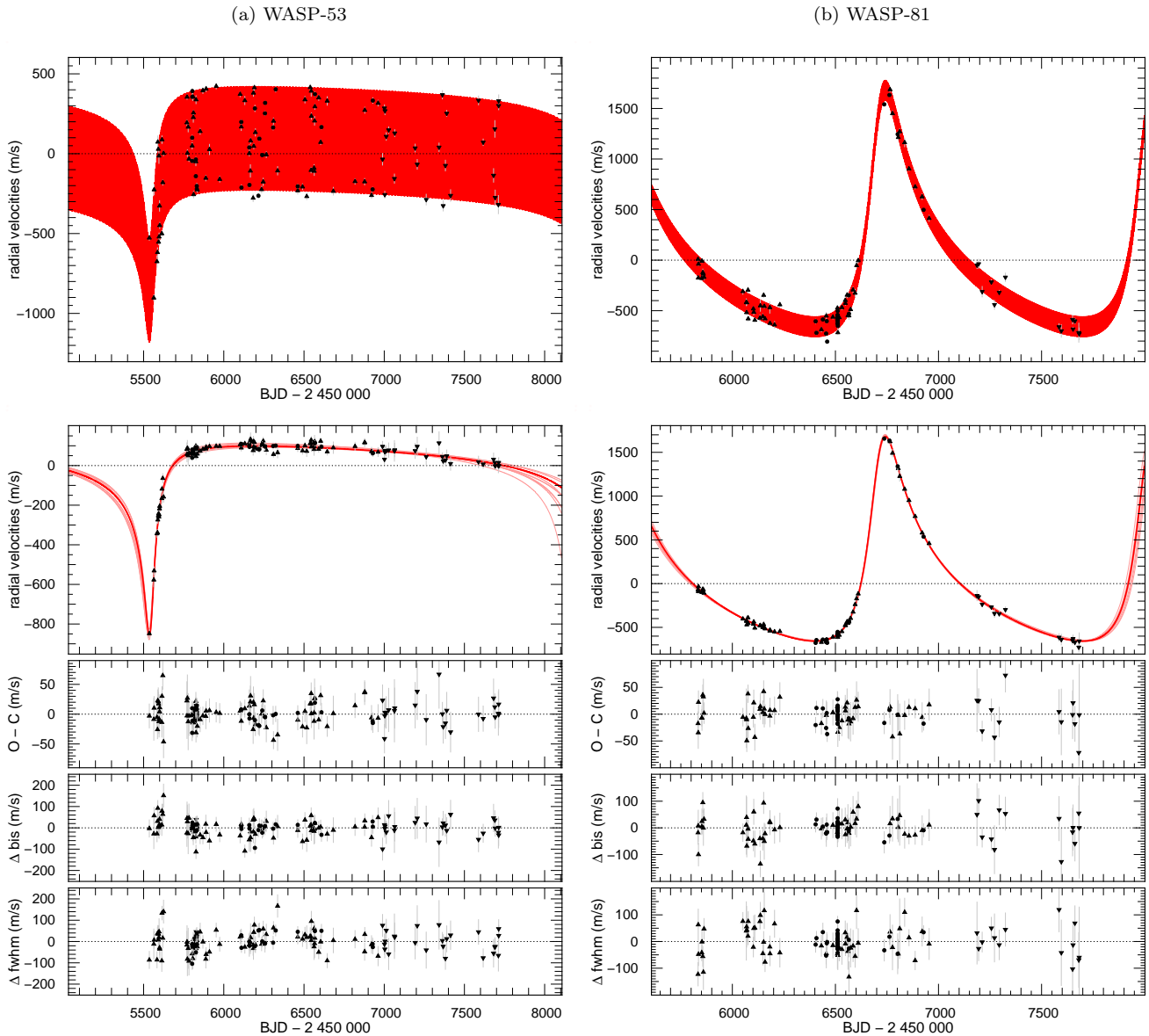


Figure 5. Radial velocities and models for WASP-53 (*left*) and WASP-81 (*right*). HARPS points are represented by discs, CORALIE is shown as triangles, pointed upwards prior to the upgrade and downwards for data acquired since. *top*: Radial velocity timeseries with the preferred two-planet model adjusted to the data. *middle*: same as on top, minus the inner planet. Ten alternative models, sampled randomly from the posterior are displayed in pink. Rossiter–McLaughlin sequences were removed from these plots; they can be found in Fig. 7. Residuals are shown below the main plots. Further down, in order, we have the variation in the slope of the bisector span, and the variation in the FWHM of the cross-correlation function.

recovered and found to be in phase. Our monitoring continued and we observed the velocity of the star rise until it plateaued, indicating that an additional, massive, highly eccentric object had just finished passing through periastron. Our observations are on-going and, to this day, the velocity of the star has yet to decrease to the level observed at our first spectrum. In total we present 98 spectra with CORALIE, including 25 since an upgrade that saw the installation of new, octagonal, fibres (Nov 2014), and of a Fabry–Pérot (Apr 2015) for the wavelength calibration throughout the night. We also gathered 83 spectra with HARPS, which include three timeseries obtained

during transit, in order to capture the Rossiter–McLaughlin effect.

The CORALIE data were divided into two independent datasets in order to account for any offset between before and after the upgrade. The HARPS set was divided into four sets, one for each Rossiter–McLaughlin effect (plus the measurement obtained the night before and after transit), and one set containing all the rest of the data. We obtained similar results by analysing the HARPS data as one set, however the division mitigates against any activity effect, such as done in [Triaud et al. \(2009\)](#). The Journal of Observations (Appendix B) is separated in several tables according to the various sub-samples of radial-velocities.

4.2.2 *WASP-81*

CORALIE acquired our first spectrum on the WASP-81 system on 2011-09-29. The following night another was observed at the opposite phase. Its radial velocity revealed a variation and the target was placed in high priority. Within a month we had confirmed a variation at the WASP photometric period, and the star had set. The following season, we intended to monitor just enough to confirm that the oscillation was still in phase and to start routine long-term monitoring, as in the case of WASP-47 (Neveu-VanMalle et al. 2016). The first measurement had a value clearly below expectations so we resumed an intense follow-up. As with WASP-53 we requested observing time on HARPS and monitored the system in parallel with CORALIE. On the third season, as we had predicted, the velocity reached a minimum and started rising. HARPS was the first instrument on sky for the fourth season. We had anticipated that the system would have returned to a similar velocity as in the first points. We were surprised to find that the star was nearly 2 km s^{-1} higher than in the previous season. Shortly after, velocities started to drop and the outer orbit closed earlier this year. In total 67 spectra were collected with CORALIE, 14 of which were after the upgrade. With HARPS we gathered 32 measurements, of which 19 were obtained during a single night as an attempt to detect the Rossiter–McLaughlin effect.

As with WASP-53 we separate the CORALIE data into two sets, before and after upgrade. Since we do not detect the R–M effect, all of the HARPS points are analysed as part of the same set. Refer to the Journal of Observations (Appendix B) for further details.

5 GLOBAL ANALYSIS

We analysed all of the photometric data and all of the radial velocity data together. We estimated the observed and physical parameters of the system using an MCMC algorithm, as detailed in Gillon et al. (2012). Our modus operandi is similar with the difference described below.

The photometric lightcurves were modelled using the formalism of Mandel & Agol (2002) for a transiting planet. The TRAPPIST and EulerCam lightcurves timestamps were transformed into BJD(TDB) from JD(UTC). The limb darkening was included in the form of a quadratic law, and its parameters were allowed to float, within the constraints of priors. The priors were computed by interpolating the data tabulated by Claret (2004), consistent with the stellar parameters of Table 2. In addition, on each photometric timeseries, we allowed for a quadratic polynomial as a function of time in order to adjust for differential extinction relative to the ensemble of comparison stars. After this treatment some lightcurves still contained a significant residual scatter. For these we tried a number of other detrending functions, selecting them on the basis of a reduction in the global Bayesian Information Criterion (BIC thereafter; Schwarz (1978)). Those comparisons were performed by systematically using the same starting seed for the random elements. Details about which functions were selected and applied can be found in Appendix C. For those lightcurves where any new degree of complexity led to a worsened BIC,

but where nevertheless the overall χ^2 implied a poor fit, we scaled³ our error bars so as to approach a general reduced $\chi_r^2 = 1$. The uncertainty increase ensures that our confidence intervals are not under-estimated. Those correction factors are available in Table C1. A similar approach is used for the radial-velocities, by quadratically adding a *jitter* term to some sequences. Two of the nine sequences required a jitter of order $1.5\text{--}2 \text{ m s}^{-1}$.

Individual detrended lightcurves and their transit model can be visually inspected in Fig. 3 & 4. Residuals and fully modelled lightcurves are presented in Appendix C.

The radial velocities around the orbit were adjusted with two eccentric Keplerian functions (as in Hilditch (2001)), neglecting Newtonian effects. Since we cover less than an orbital period for WASP-53c and barely one for WASP-81c, we did not include a long term trend. Its inclusion leads to higher BIC values and its slope is mostly unconstrained. The Rossiter–McLaughlin effect was computed using the code written by Giménez (2006), following the formalism of Kopal (1942). For WASP-81b the effect was not detected and the final fit does not include it. For both systems we find the inner planets’ orbits to be consistent with circular. Although allowing for eccentricity adds two parameters and increases the BIC, we nevertheless let these parameters float so as to include their uncertainties when marginalising the other parameters.

The MCMC’s jump parameters are mostly set to match observables, which are then converted to physical parameters to compute the relevant models. D is the transit depth, b the impact parameter, W the transit width. T_0 is the mid-transit time and P the orbital period. We combine, the eccentricity e and the angle of periastron ω into the pair $\sqrt{e} \cos \omega$, $\sqrt{e} \sin \omega$ which helps when exploring small eccentricities (Triaud et al. 2011). Similarly we also construct the pair $\sqrt{v} \sin I_\star \cos \beta$, $\sqrt{v} \sin I_\star \sin \beta$ to model the Rossiter–McLaughlin effect. β is the projected spin–orbit angle, and $v \sin I_\star$ the measure of the projected rotation velocity of the star, which in principle should match $v \sin i_\star$ from the spectral analysis. Instead of the semi-amplitude K we use the jump parameter K_2 such that $K_2 = K\sqrt{1 - e^2 P^{1/3}}$. This helps reduce some correlation between the parameters (Ford 2006) helping with the exploration of parameter space. For similar reasons we combine the limb-darkening coefficients into $c_1 = 2u_1 + u_2$, and $c_2 = u_1 - 2u_2$ following the recommendation of Holman et al. (2006). In the case of two *Euler* lightcurves for WASP-53 we also fit a sine function through the data, with a period P and a T_0 . Additional subscript indicate which lightcurves those are for.

All jump parameters are well constrained within one scale. Except for P_c and $K_{2,c}$, we sample our parameters’ posteriors using Gaussian priors, whose variance is set with an initial Gibbs sampler. As an improvement over Gillon et al. (2012) P_c and $K_{2,c}$ were sampled using non-informative priors in log space, otherwise known as *Jeffrey* priors. However their values remained largely within one error bar, and the application of Gaussian steps does not lead to qualitatively different results. The metallicity [Fe/H], and

³ we realise that this approach is not self-consistent, but our method is sufficient for small re-adjustments of the uncertainties and unambiguous detections.

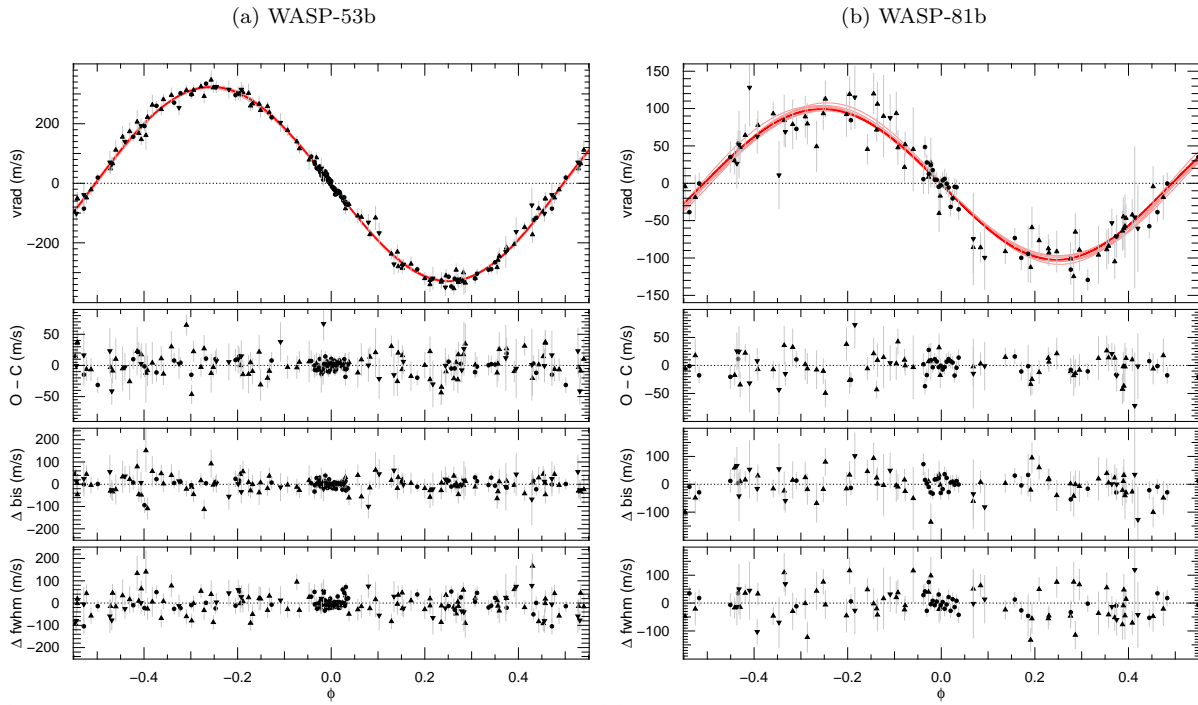


Figure 6. Radial velocity measurements phased with the orbit of the inner planet, after subtracting the variation due to the outer object. The preferred model is drawn in thick red, with another ten alternate models randomly picked from the posterior shown in pink. Residuals are shown below the main plots. Further down we have the variation in the slope of the bisector span, and the variation in the FWHM of the cross-correlation function. The symbols are as in Fig. 5.

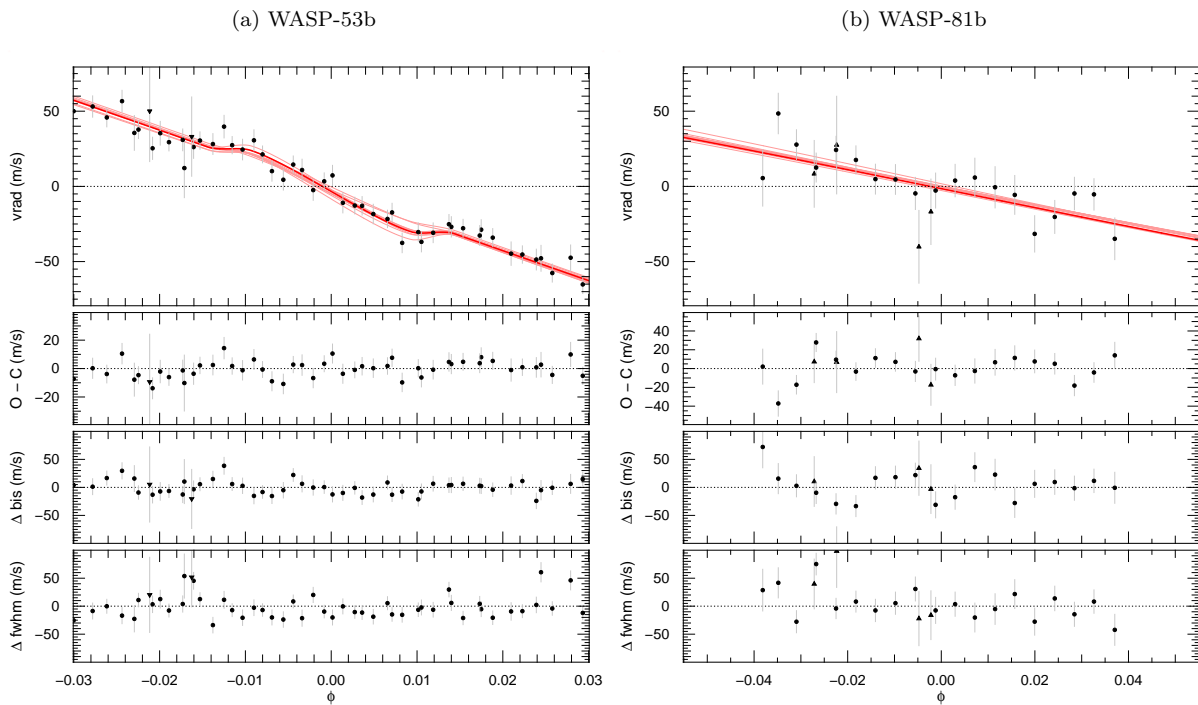


Figure 7. As for Fig. 6 but zoomed around transit time to show the Rossiter–McLaughlin effect.

Table 3. Median and 1σ confidence regions for the jump parameters that evolve in our MCMC chains. Errors on the last two digits of each parameters are given in brackets. Parameters not dependent on information contained within the adjusted data are highlighted with asterisks

Parameters (Units)	WASP-53	WASP-81	
<i>the star</i>			
[Fe/H] (dex)	0.22 ^(+0.11) _(-0.11)	-0.36 ^(+0.14) _(-0.14)	*
T_{eff} (K)	4953 ⁽⁺⁵⁹⁾ ₍₋₆₀₎	5870 ⁽⁺¹²⁰⁾ ₍₋₁₂₀₎	*
$c_{1,JR}$	-	0.918 ⁽⁺³³⁾ ₍₋₃₃₎	*
$c_{2,JR}$	-	-0.280 ⁽⁺²³⁾ ₍₋₂₃₎	*
$c_{1,BB}$	1.069 ⁽⁺³⁷⁾ ₍₋₃₈₎	0.772 ⁽⁺⁵⁷⁾ ₍₋₅₇₎	*
$c_{2,BB}$	0.031 ⁽⁺³¹⁾ ₍₋₃₀₎	-0.321 ⁽⁺³⁷⁾ ₍₋₃₈₎	*
$c_{1,I+z}$	0.995 ⁽⁺⁶²⁾ ₍₋₆₁₎	0.807 ⁽⁺⁵⁵⁾ ₍₋₅₇₎	*
$c_{2,I+z}$	-0.020 ⁽⁺³⁷⁾ ₍₋₃₇₎	-0.297 ⁽⁺³⁰⁾ ₍₋₃₂₎	*
$c_{1,r'}$	1.316 ⁽⁺²⁹⁾ ₍₋₂₉₎	-	*
$c_{2,r'}$	0.272 ⁽⁺²⁸⁾ ₍₋₂₈₎	-	*
<i>inner planet</i>			
D_b	0.01831 ⁽⁺³³⁾ ₍₋₃₄₎	0.01254 ⁽⁺²⁷⁾ ₍₋₂₆₎	
b_b (R_\odot)	0.562 ⁽⁺²⁰⁾ ₍₋₂₂₎	0.15 ^(+0.10) _(-0.10)	
W_b (d)	0.09469 ⁽⁺⁶⁵⁾ ₍₋₆₄₎	0.14501 ⁽⁺⁷³⁾ ₍₋₆₄₎	
$T_{0,b}$ (BJD -2 450 000)	5943.56695 ⁽⁺¹¹⁾ ₍₋₁₂₎	6195.57462 ⁽⁺²⁰⁾ ₍₋₂₀₎	
P_b (d)	3.3098443 ⁽⁺²⁰⁾ ₍₋₂₀₎	2.7164762 ⁽⁺²³⁾ ₍₋₂₃₎	
$\sqrt{e_b} \cos \omega_b$	-0.070 ⁽⁺²⁴⁾ ₍₋₂₁₎	-0.026 ⁽⁺⁸³⁾ ₍₋₇₆₎	
$\sqrt{e_b} \sin \omega_b$	-0.085 ⁽⁺⁴⁶⁾ ₍₋₃₃₎	-0.00 ^(+0.12) _(-0.12)	
$K_{2,b}$ ($ms^{-1}d^{1/3}$)	485.9 ^(+2.7) _(-2.7)	140.7 ^(+4.7) _(-4.6)	
$\sqrt{v \sin I_\star} \cos \beta_b$	0.91 ^(+0.11) _(-0.13)	-	
$\sqrt{v \sin I_\star} \sin \beta_b$	-0.07 ^(+0.19) _(-0.19)	-	
<i>outer planet</i>			
$T_{0,c}$ (BJD -2 450 000)	5456 ⁽⁺¹¹⁾ ₍₋₁₃₎	6936.5 ^(+2.6) _(-2.5)	
P_c (day)	2840 ⁽⁺¹⁷⁰⁾ ₍₋₁₃₀₎	1297.2 ^(+8.1) _(-7.8)	
$\sqrt{e_c} \cos \omega_c$	-0.867 ⁽⁺¹²⁾ ₍₋₁₂₎	0.5871 ⁽⁺⁴⁰⁾ ₍₋₄₂₎	
$\sqrt{e_c} \sin \omega_c$	-0.292 ⁽⁺³⁰⁾ ₍₋₃₀₎	-0.4609 ⁽⁺⁶¹⁾ ₍₋₆₁₎	
$K_{2,c}$ ($ms^{-1}d^{1/3}$)	3685 ⁽⁺¹¹⁰⁾ ₍₋₈₉₎	10 557 ⁽⁺⁵¹⁾ ₍₋₅₀₎	
jump parameters:	23	21	

effective temperature T_{eff} complete this list of jump parameters. They are controlled by priors obtained from Table 2 and used to compute at every MCMC step a stellar mass and a stellar radius produced in a fashion similar to Torres, Andersen & Giménez (2010).

For our final analysis we set 10 chains of 100 000 steps, starting from different seeds. All converged to similar BIC values. The first 20 000 steps were systematically removed (to allow for burn-in), and the remainder were analysed leading to our results. For each of our 10 chains we extract the median value for each parameter and compare them to one another. They are usually of order 0.1% different from one another, except for the jump parameters responsible for modelling WASP-53c, which can vary as much as 60%. This is because the orbit is not closed. We discuss this further in the next section.

Table 4. Final estimates for the median and 1σ confidence regions, for various interesting parameters of the WASP-53 and WASP-81 systems. They were estimated from the posteriors of the jump parameters outlined in Table 3. Errors on the last two digits of each parameters are given in brackets. Upper limits are for 3σ confidence. Parameters not dependent on information contained within the adjusted data are highlighted with asterisks

Physical Parameters	WASP-53	WASP-81	
<i>the star</i>			
M_\star (M_\odot)	0.839 ⁽⁺⁵⁴⁾ ₍₋₅₄₎	1.080 ⁽⁺⁵⁹⁾ ₍₋₅₈₎	*
R_\star (R_\odot)	0.798 ⁽⁺²³⁾ ₍₋₂₃₎	1.283 ⁽⁺⁴⁰⁾ ₍₋₃₇₎	
ρ_\star (ρ_\odot)	1.648 ⁽⁺⁹¹⁾ ₍₋₈₅₎	0.513 ⁽⁺³⁰⁾ ₍₋₃₇₎	
L_\star (L_\odot)	0.344 ⁽⁺²³⁾ ₍₋₂₃₎	1.76 ^(+0.20) _(-0.18)	
T_{eff} (K)	4953 ⁽⁺⁶⁰⁾ ₍₋₆₀₎	5870 ⁽⁺¹²⁰⁾ ₍₋₁₂₀₎	*
$\log g_\star$ (cgs)	4.553 ⁽⁺¹⁹⁾ ₍₋₂₀₎	4.258 ⁽⁺²²⁾ ₍₋₂₇₎	*
[Fe/H] (dex)	0.22 ^(+0.11) _(-0.11)	-0.36 ^(+0.14) _(-0.14)	*
$v \sin I_\star$ ($km s^{-1}$)	0.86 ^(+0.21) _(-0.21)	-	
<i>inner planet</i>			
P_b (day)	3.3098443 ⁽⁺²⁰⁾ ₍₋₂₀₎	2.7164762 ⁽⁺²³⁾ ₍₋₂₃₎	
$T_{0,b}$ (BJD -2 450 000)	5943.56695 ⁽⁺¹¹⁾ ₍₋₁₂₎	6195.57462 ⁽⁺²³⁾ ₍₋₂₀₎	
K_b ($m s^{-1}$)	326.1 ^(+1.8) _(-1.8)	100.8 ^(+3.4) _(-3.3)	
M_b (M_{Jup})	2.132 ⁽⁺⁹²⁾ ₍₋₉₄₎	0.729 ⁽⁺³⁶⁾ ₍₋₃₅₎	
R_b (R_{Jup})	1.074 ⁽⁺³⁷⁾ ₍₋₃₇₎	1.429 ⁽⁺⁵¹⁾ ₍₋₄₆₎	
ρ_b (ρ_{Jup})	1.72 ^(+0.15) _(-0.13)	0.250 ⁽⁺²³⁾ ₍₋₂₃₎	
$\log g_b$ (cgs)	3.680 ⁽⁺²²⁾ ₍₋₂₂₎	2.967 ⁽⁺²⁷⁾ ₍₋₃₀₎	
a_b/R_\star	11.05 ^(+0.20) _(-0.19)	6.56 ^(+0.13) _(-0.16)	
$T_{b,\text{eq}}$ (K)	1053 ⁽⁺¹⁶⁾ ₍₋₁₆₎	1623 ⁽⁺³⁸⁾ ₍₋₃₇₎	
a_b (AU)	0.04101 ⁽⁺⁸³⁾ ₍₋₉₁₎	0.03908 ⁽⁺⁷⁰⁾ ₍₋₇₂₎	
i_b (deg)	87.08 ^(+0.16) _(-0.15)	88.69 ^(+0.88) _(-0.92)	
β_b (deg)	-4 ⁽⁺¹²⁾ ₍₋₁₂₎	-	
e_b	< 0.030	< 0.066	
<i>outer planet</i>			
P_c (day)	> 2840 ⁽⁺¹⁷⁰⁾ ₍₋₁₃₀₎	1297.2 ^(+8.1) _(-7.8)	
$T_{0,c}$ (BJD -2 450 000)	5456 ⁽⁺¹¹⁾ ₍₋₁₃₎	6936.5 ^(+2.6) _(-2.5)	
K_c ($m s^{-1}$)	> 475.6 ^(+8.2) _(-8.0)	1169.3 ^(+6.9) _(-6.6)	
$M_c \sin i_c$ (M_{Jup})	> 16.35 ^(+0.85) _(-0.82)	56.6 ^(+2.0) _(-2.0)	
a_c (AU)	> 3.73 ^(+0.16) _(-0.14)	2.426 ⁽⁺⁴⁴⁾ ₍₋₄₅₎	
e_c	0.8369 ⁽⁺⁶⁹⁾ ₍₋₇₀₎	0.5570 ⁽⁺⁴⁴⁾ ₍₋₄₄₎	
ω_c (deg)	198.6 ^(+2.0) _(-2.0)	321.86 ^(+0.52) _(-0.51)	

The posterior probability distributions have been stored and can be requested by email to the lead author. We present the median values and 1σ region of our posteriors in Table 3 for the jump parameters, and in Table 4 for the physical parameters. The results are discussed in the following section.

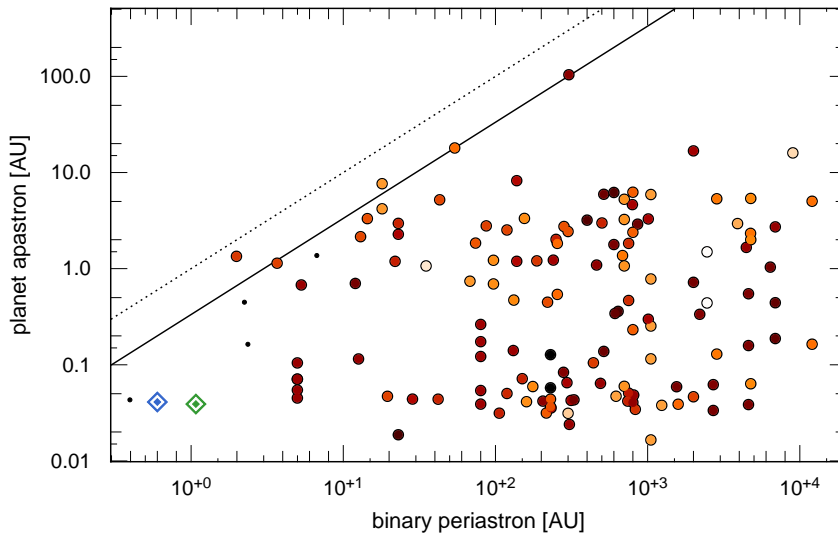


Figure 8. Planetary apastron versus binary periastron (or separation if eccentricity is unknown) in astronomical units for known S-type planetary systems. The colour of the dots reflects the logarithm of the ratio of the planet-hosting star mass to the mass of its stellar companion(s) (white = 0.2, black = 18). WASP-53 and WASP-81 are highlighted as a blue and green diamond, respectively. The small black dots represent four systems containing a gas-giant and a brown dwarf. The dotted line is a 1:1 line, and the plain line is a 3:1 contour. Above that line systems are usually unstable (Dvorak 1986; Holman & Wiegert 1999). Data collected from openexoplanetcatalogue.com, from www.univie.ac.at/adg/schwarz/multiple.html, and from exoplanet.eu.

6 RESULTS

6.1 WASP-53

WASP-53 is a system composed of a star and two orbiting objects. WASP-53b is a hot Jupiter with a mass $M_b = 2.1 \pm 0.1 M_{\text{Jup}}$, with a radius $R_b = 1.07 \pm 0.04 R_{\text{Jup}}$. We find the inner orbit to be consistent with zero eccentricity, placing a 99% confidence limit of 0.03. The Rossiter–McLaughlin effect is weakly detected. We find a lower amplitude than we anticipated, likely because $v \sin i_*$ is over-estimated owing to an under-estimation of macroturbulence, as already noted for a number of late-type dwarfs (e.g. Triaud et al. (2011, 2015)). We find the spin–orbit angle $\beta = -4^\circ \pm 12$. The planet appears to be coplanar.

The orbit of WASP-53c does not close within the span of our observations, which affects the various chains we launched. The median values on individual jump parameters values can vary by as much as 50%, which is reflected in the large errors in Table 3 and 4. This means that while we provide median values and their 1σ confidence ranges, those are in fact more akin to lower limits on M_c , e_c , P_c etc. WASP-53c is at least $16 M_{\text{Jup}}$, with a period likely longer than 2500 days. The eccentricity of its orbit is high with our data being most consistent with 0.84 ± 0.01 .

We were lucky to observe the system during the final phases of WASP-53c’s periastron passage (but unlucky to miss the first half). If removing the first season of CORALIE data, we only detect a quadratic drift with a weak curvature and would never have guessed the presence of such a massive companion within the system.

6.2 WASP-81

WASP-81 is a system composed of a star and two orbiting objects. WASP-81b is a hot Jupiter whose mass is $M_b =$

Table 5. Dates on which WASP-53c and WASP-81c may transit. Numbers are calendar dates and Barycentric Julian Dates (BJD) – 2 450 000.

WASP-53c	WASP-81c
<i>passed dates</i>	
–	3044.9 ⁺²⁴ _{–24} (2004-02-09)
–	4342.1 ⁺¹⁶ _{–16} (2007-08-29)
2616.0 ⁺¹⁷⁰ _{–130} (2002-12-07)	5639.3 ^{+8.5} _{–8.2} (2011-03-18)
5455.5 ⁺¹¹ _{–13} (2010-09-16)	6936.5 ^{+2.6} _{–2.5} (2014-10-06)
<i>future dates</i>	
8295.1 ⁺¹⁷⁰ _{–130} (2018-06-25)	8233.8 ^{+8.5} _{–8.2} (2018-04-25)
–	9531.0 ⁺¹⁶ _{–16} (2021-11-12)

$0.73 \pm 0.04 M_{\text{Jup}}$ and radius $R_b = 1.43 \pm 0.05 R_{\text{Jup}}$. Its orbit is consistent with being circular and we place a 99%-confidence upper limit at 0.07. The Rossiter–McLaughlin effect is not detected. Its amplitude is projected to be less than 10 m s^{-1} . The low impact parameter means that the spin–orbit angle will be degenerate with $v \sin i_*$ as in Triaud et al. (2011).

WASP-81c has a minimum mass $M_c = 57 \pm 2 M_{\text{Jup}}$, a period $P_c = 1297 \pm 8$ days and an eccentricity of order 0.56.

7 DISCUSSION

We have discovered two hot Jupiters orbiting the primary star of two tight binary systems. WASP-53b is super-Jupiter in mass, while WASP-81b is sub-Jupiter. Both occupy orbits that are typical for hot Jupiters (eg. Santerne et al. 2016). Those two planets are both accompanied by brown-dwarf-mass objects, on highly eccentric orbits of a few AU. In Fig. 8, we plot other known planetary systems orbiting

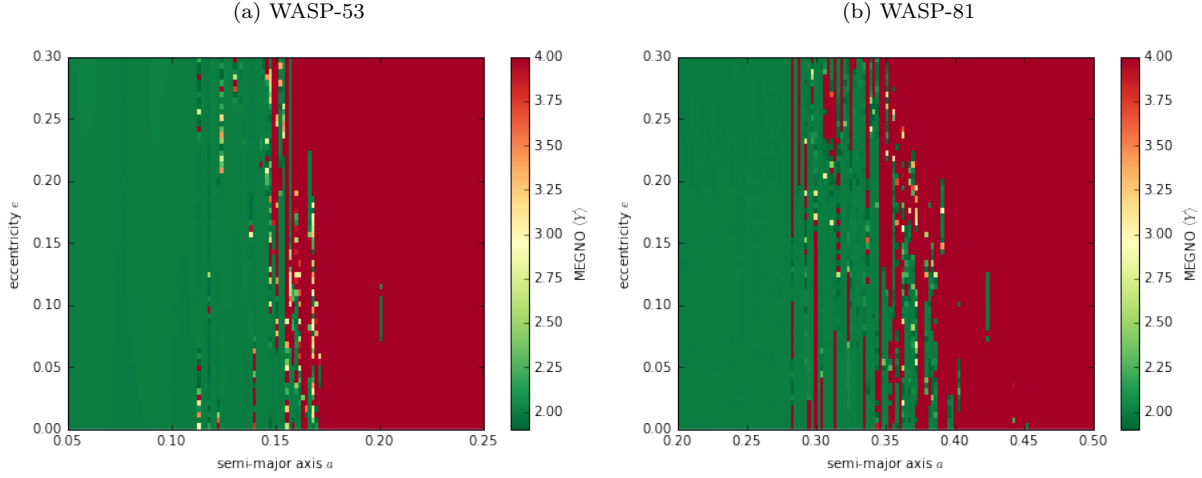


Figure 9. MEGNO maps showing regions of stability in green, and chaos in red, showing where planets with the masses of WASP-53b and WASP-81b could exist. Any value in excess of 4 has the same colour. All regions on the left-hand side of the graphs are stable, and all regions on the right-hand side are unstable (within the outer orbit). Maps computed by integrating for 5×10^4 years

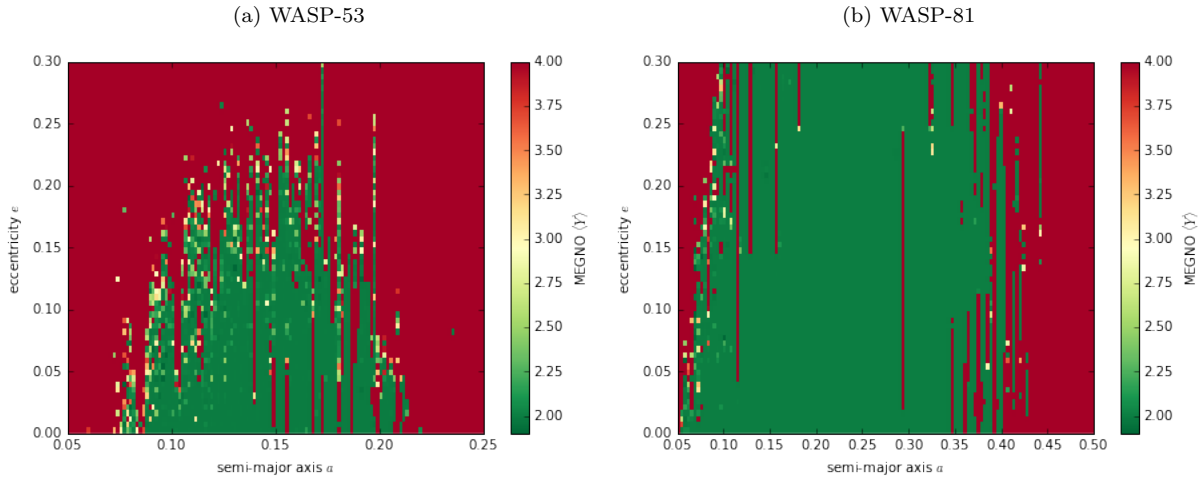


Figure 10. MEGNO maps showing regions of stability in green, and chaos in red, for mass-less particles between the positions of the inner and outer objects in the WASP-53 and WASP-81 systems. Any value in excess of 4 has the same colour. Maps computed by integrating for 5×10^4 years

one star of a multiple stellar system, showing how atypical WASP-53 and WASP-81 are within the current exoplanet population. Only four other systems have a stellar companion with periastra closer than 10 AU: Kepler-444 (Dupuy et al. 2016), KOI-1257 (Santerne et al. 2014), HD 59686 (Ortiz et al. 2016) and the astonishing, maybe retrograde, ν Oct (Ramm 2015) (the leftmost red dot, above the plain line). In addition, four gas giants have outer brown-dwarf companions: HAT-P-13 (Knutson et al. 2014), HIP 5158 (Feroz, Balan & Hobson 2011), HD 168443 (Sahlmann et al. 2011), and HD 38529 (Benedict et al. 2010), in architectures similar to WASP-53 and WASP-81.

We now review the elements that make those systems stand out. We speculate about their origin, and propose some observational tests to verify some of our scenarios.

We use the stability criterion numerically determined by Holman & Wiegert (1999) to compute the widest orbital

separation that each of the hot Jupiters could have occupied. In the case of WASP-53 we obtain a critical semi-major axis $a_{\text{crit}} = 0.16 \pm 0.15$ AU, and for WASP-81, $a_{\text{crit}} = 0.38 \pm 0.06$ AU. This criterion was numerically determined for a mass ratio $\mu = m_2/(m_1 + m_2) > 0.1$, which is not satisfied for either of our systems, and likely explains the large uncertainty for WASP-53. We therefore proceed with a stability criterion devised by Petrovich (2015b) for hierarchical planetary system. We find that unstable orbit start emerging for $0.14 < a_b < 0.17$ for WASP-53, and $0.30 < a_b < 0.38$ for WASP-81, in good agreement with the previous approach.

We further verify this with the method proposed by Cincotta, Giordano & Simó (2003), which uses a marker called the MEGNO (the Mean Exponential Growth factor of Nearby Orbits), as implemented in REBOUND by Rein & Tamayo (2015). The MEGNO is a good tracker of orbital chaos, meaning that infinitesimal changes in initial pa-

rameters lead to diverging solutions. For quasi-periodic orbits, thus those showing no chaotic behaviour, the MEGNO reaches a value of 2 (Hinse et al. 2010). Larger values of the MEGNO, typically > 4 , indicate significant changes in the orbital parameters, a sign of chaos. Although this does not necessarily translate by unstable orbits (e.g. Deck et al. 2012), it often tracks them as we saw above. For our case the MEGNO outlines where nearly closed orbits exist and therefore informs us on where any disc material may have been stable, or where additional planets may exist.

We used the parameters provided in Tab. 4 for the outer companions, assumed coplanarity between the inner and outer orbits, and computed the MEGNO for a particle with a mass and separation for WASP-53b and WASP-81b. We integrated each system for 5×10^6 years and obtained values of 2.0062 and 1.9999 respectively, indicating stability. We expanded those simulation and explore the (a, e) parameter space. To compute the maps presented in Fig. 9 we integrated each of the pixels over 5×10^4 years. We observe from those results that wide regions of chaos exist, which is consistent with the work of Holman & Wiegert (1999) and Petrovich (2015b). Both WASP-53 and WASP-81 appear stable over long periods of time. In the case of WASP-53 we observe that only regions closer in than 0.15 AU retain stable orbits. For WASP-81 there is slightly more space with orbits within 0.3 AU being generally stable.

We also investigated whether other planets could exist between objects b and c by adding a third massless particle. The results are displayed in Fig. 10, which show a range of stable orbits (in green). While this suggests that other planets could still be identified within our systems, we think it unlikely since hot Jupiters are usually found to be isolated. Only one hot Jupiter is known to have other planetary companions within an astronomical unit (Becker et al. 2015; Neveu-VanMalle et al. 2016), and a recent analysis of the *Kepler* data shows that a lack of nearby companions is an important aspect that sets hot Jupiters apart from other gas giants (Huang, Wu & Triaud 2016).

7.1 Determination of the mass and orbital inclination of WASP-53c and WASP-81c

Gaia (Perryman et al. 2001) is an ESA mission launched in 2013 currently scanning the sky and measuring stellar positions with a precision of order 30 micro-arcseconds for stars brighter than optical magnitude 12 (de Bruijne 2012). Several studies have investigated *Gaia*'s potential for detecting gas giants using astrometry (Casertano et al. 2008; Sozzetti et al. 2014; Perryman et al. 2014; Sahlmann, Triaud & Martin 2015), with Neveu et al. (2012) looking into the combination of radial-velocities with astrometric measurements.

From Perryman et al. (2014), WASP-53c and WASP-81c will produce an astrometric displacement of their host stars, α , defined as:

$$\alpha = \left(\frac{M_p}{M_\star}\right) \left(\frac{a}{1\text{AU}}\right) \left(\frac{d}{1\text{pc}}\right)^{-1} \text{ arcsec} \quad (1)$$

WASP-53 and WASP-81 will move on the sky by $\alpha = 260$, and $300 \mu\text{as}$ respectively, caused by their outer companions, assuming an orbital inclination $i_c = 90^\circ$, which is the poorest scenario possible. We can expect of order

$N_{\text{obs}} = 70$ astrometric measurements⁴ with typical uncertainties $\sigma = 40 \mu\text{as}$ (de Bruijne 2012) to be collected on our two targets. This translates to an astrometric signal-to-noise, where $S/N = \alpha\sqrt{N_{\text{obs}}}/\sigma$, in excess of 50 for both systems. If instead $i_c = 10^\circ$, we obtain $\alpha = 1500$, and $1700 \mu\text{as}$ respectively⁵. The amplitude of the orbital motion alone should inform us of the mutual inclination between the inner and outer planet. For astrometric signal-to-noise values of > 20 the orbital inclination will typically be estimated with a precision of $< 10^\circ$ (Sahlmann, Triaud & Martin 2015).

7.2 Transit timing variations

Using REBOUND (Rein & Spiegel 2015) we integrated the system over a few orbital periods of the outer companion and recorded when transits of the inner planet happened. For WASP-53b we expect total transit-timing variations, caused by the perturbing effect of the outer companion, to be of order 35s. However, most of the variation happens during periastron, which means that during nearly 100 transit epochs we covered for WASP-53b, we expect no variation to be measurable). We expect a detectable signal to appear within the next two years if our solution for the outer companion is correct. After WASP-53c swings again via periastron, the ephemeris for WASP-53b will become offset by approximately 35s. This offset remains constant until the following periastron when it will offset again by the same amount. We repeated the procedure for WASP-81 and find a similar TTV behaviour for WASP-81b with offset of approximately 30s compared to the value we produce here.

7.3 Estimating k_2

Secular interactions between pairs of orbiting planets usually excites their orbital eccentricities. In the case of WASP-53 and WASP-81, the innermost planetary orbit will be affected by tidal forces which tend to damp eccentricity, while the outer, massive companion occupies a highly eccentric orbit which will excite the inner planet's eccentricity. Mardling (2007) investigated this secular problem and found that the inner planet will reach an equilibrium eccentricity, called a *fixed-point*, with a value dependent on the planet's internal density profile, and parametrised by k_2 , the tidal Love number (Sterne 1939). The more mass that gets included into the core of the planet, the larger will be the fixed-point eccentricity (Batygin, Bodenheimer & Laughlin 2009). As such a measure of the eccentricity of the tidally damped, inner orbit can yield the core-mass fraction of exoplanets. Recently, Buhler et al. (2016) investigated the case of the HAT-P-13 system that presents an architecture similar to WASP-53 and WASP-81, and managed to constrain the core mass of the transiting hot Jupiter to $11 M_\oplus$ by measuring an eccentricity of 0.007 ± 0.001 . We see here how our two systems compare.

We estimated the inner eccentricity, first assuming

⁴ 78 expected measurements for WASP-53, and 60 for WASP-81 according to the following tool: <http://gaia.esac.esa.int/gost/>

⁵ we do not detect a secondary set of lines in either of our spectra. This is equivalent to a limit of $i_c > 2^\circ$, and $i_c > 5^\circ$ respectively.

no tidal damping, using eq. 36 in [Mardling \(2007\)](#), and found fixed-point eccentricities of 0.00053 for WASP-53b, and 0.0027 for WASP-81b (HAT-P-13's parameters yield 0.0087). Any tidal dissipation will reduce these values by an amount dependent on the internal composition. Similarly, any mutual inclination between the outer and inner orbits will reduce these values. Sadly, because the eccentricities we expect of WASP-53b and WASP-81b are so small, we find it unlikely that their internal composition will be determined soon. If however, the eccentricity is one day measured, we should expect apsidal alignment or anti-alignment between the inner and outer orbits. The Love number can also be extracted from the way a transit lightcurve gets affected by apsidal precession ([Ragozzine & Wolf 2009](#)).

7.4 Possible scenarios for the planets' formation and orbital evolution

We here speculate about the sequence of events leading to systems like WASP-53 and WASP-81, and also to HAT-P-13b ([Bakos et al. 2009](#)), HD 59686Ab ([Ortiz et al. 2016](#)) and others. The presence of both a planet and a brown-dwarf mass object (one on the planetary side, the other on the stellar side of the brown-dwarf desert; [Grether & Lineweaver 2006](#); [Sahlmann et al. 2011](#)) within the same system possibly suggests that core accretion and gravitational collapse can both operate within the same disc environment. They may also be smaller fragments from the nebula that created WASP-53A and WASP-81A.

Both WASP-53b and WASP-81b could initially have formed on circumbinary orbits, to be captured by the primary following a dynamical instability. This sort of scenario has been investigated by [Sutherland & Fabrycky \(2016\)](#), and shown to be an unlikely outcome, which, when it does happen, favours capture of the planet by the secondary instead of the primary. Therefore, WASP-53b and WASP-81b most likely formed within a disc surrounding WASP-53A and WASP-81A.

We can think of two alternate scenarios and make an appeal for theorists to investigate them since they could teach us much about how gas giants form.

WASP-53c and WASP-81c are too massive compared to the protoplanetary disc to have followed a type-II migration ([Duffell et al. 2014](#); [Dürmann & Kley 2015](#)). If no or little orbital evolution has happened within the two systems that we studied, then WASP-53b and WASP-81b must have formed well within the snow line, on orbits shorter than 0.15 and 0.3 AU respectively. Theoretical work by [Batygin, Bodenheimer & Laughlin \(2015\)](#) and [Lee & Chiang \(2015\)](#) suggests that the formation of gas giants within one astronomical unit is feasible. According to [Fung, Shi & Chiang \(2014\)](#) gas can flow through the gap carved by a planet, particularly so if it reaches masses near that of a brown dwarf. The more massive the object, the more perturbations are produced at the outer gap's edge, launching streams of gas that replenish the inner disc to provide enough mass to allow the formation of a gas giant. The large eccentricities of WASP-53c and WASP-81c might have enhanced this effect. However, [Lambrechts, Johansen & Morbidelli \(2014\)](#) and [Rosotti et al. \(2016b\)](#) find that planets more massive than 20–30 Earth masses prevent the flow of dust grains across the same gap. Accordingly, if WASP-53b and WASP-

81b formed in-situ via core-accretion, they could only have used solids within about 0.2 AU, before being able to accrete gas. If this scenario is correct, systems like WASP-53 and WASP-81 can inform us about the efficiency of core accretion, as well the minimum core mass necessary to accrete significant gas envelopes. This would also leave the planets poorer in metals than otherwise, something which is possible to determine via transmission spectroscopy ([Seager & Deming 2010](#); [Madhusudhan et al. 2014](#))

WASP-53c and WASP-81c are both eccentric. It has been argued that disc-planet interactions can excite the eccentricity of gap-opening planets, but not to the values that we observe for WASP-53c and WASP-81c (e.g. [Goldreich & Sari 2003](#); [D'Angelo, Lubow & Bate 2006](#); [Rosotti et al. 2016a](#); [Teyssandier & Ogilvie 2016](#)). This might imply that WASP-53c and WASP-81c reached their current orbital parameters after disc dispersal, possibly due to dynamical interactions with third, yet unseen companions to WASP-53 and WASP-81. If this is the case then either WASP-53b and WASP-81b disc-migrated well before WASP-53c and WASP-81c reached their current orbits, or, WASP-53b and WASP-81b reached their current orbit following a high-eccentricity migration produced by the same instability that left their outer companions on eccentric orbital paths. In either of those cases, we expect a significant mutual inclination between the inner and outer orbits, which *Gaia* should in principle be able to measure. Coplanarity would favour the scenario outlined in the previous paragraph.

8 CONCLUDING WORDS

WASP-53 & WASP-81 are peculiar systems composed of both a planet and a brown dwarf. This orbital set-up is a relic of its past formation. Investigating them in further studies, notably with the help of *Gaia*, will prove invaluable for understanding planet formation and the subsequent orbital evolution, but also the relation between planet formation, brown dwarf formation and stellar formation.

NOTA BENE

Dates are given in the BJD-TDB standard. The radii we used for Jupiter and the Sun are the volumetric mean radii.

For clarity, we used the subscripts \star for the star, b for the inner planet, and c for the outer object, all throughout.

ACKNOWLEDGMENTS

AT would like to acknowledge inspiring discussions with the following people: Rosemary Mardling, Hanno Rein, Simon Hodgkin, Daniel Tamayo, Richard Booth, Cristobal Petrovich, Yanqin Wu, Kaitlin Kratter, Jean Teyssandier, Ari Silburt and David Martin.

TRAPPIST is a project funded by the Belgian Fund for Scientific Research (Fond National de la Recherche Scientifique, F.R.S-FNRS) under grant FRFC 2.5.594.09.F, with the participation of the Swiss National Science Foundation (SNF). The *Euler* Swiss telescope is supported by the Swiss National Science Foundation. We are all very grateful to ESO and its La Silla staff for their continuous support.

WASP-South is hosted by the South African Astronomical Observatory while SuperWASP-North is hosted by the Issac Newton Group at the Observatorio del Roque de los Muchachos on La Palma. We are grateful for the ongoing support and assistance of these observatories.

M. Gillon and E. Jehin are Research Associates at the F.R.S-FNRS; L. Delrez received the support of the F.R.I.A. fund of the FNRS.

This publication makes use of data products from 2MASS, whose data was obtained through [Simbad](#) and [VizieR](#) services hosted at the [CDS-Strasbourg](#). The Two Micron All Sky Survey is a joint project of the University of Massachusetts and the Infrared Processing and Analysis Center/California Institute of Technology, funded by the National Aeronautics and Space Administration and the National Science Foundation.

References to exoplanetary systems were obtained through the use of the paper repositories, [ADS](#) and [arXiv](#), but also through frequent visits to the [exoplanet.eu](#) ([Schneider et al. 2011](#)) and [exoplanets.org](#) ([Wright et al. 2011](#)) websites.

REFERENCES

- Albrecht S., Winn J. N., Butler R. P., Crane J. D., Shectman S. A., Thompson I. B., Hirano T., Wittenmyer R. A., 2012a, *ApJ*, 744, 189
- Albrecht S. et al., 2012b, *ApJ*, 757, 18
- Alibert Y., Mousis O., Mordasini C., Benz W., 2005, *ApJL*, 626, L57
- Anderson D. R. et al., 2010, *ApJ*, 709, 159
- , 2015, *ApJL*, 800, L9
- Asplund M., Grevesse N., Sauval A. J., Scott P., 2009, *ARA&A*, 47, 481
- Bakos G. Á. et al., 2009, *ApJ*, 707, 446
- Baranne A. et al., 1996, *A&AS*, 119, 373
- Baruteau C. et al., 2014, *Protostars and Planets VI*, 667
- Batygin K., 2012, *Nature*, 491, 418
- Batygin K., Bodenheimer P., Laughlin G., 2009, *ApJL*, 704, L49
- Batygin K., Bodenheimer P. H., Laughlin G. P., 2015, *ArXiv e-prints*
- Becker J. C., Vanderburg A., Adams F. C., Rappaport S. A., Schwengeler H. M., 2015, *ApJL*, 812, L18
- Benedict G. F., McArthur B. E., Bean J. L., Barnes R., Harrison T. E., Hatzes A., Martioli E., Nelan E. P., 2010, *AJ*, 139, 1844
- Bodenheimer P., Hubickyj O., Lissauer J. J., 2000, *Icarus*, 143, 2
- Buhler P. B., Knutson H. A., Batygin K., Fulton B. J., Fortney J. J., Burrows A., Wong I., 2016, *ApJ*, 821, 26
- Casertano S. et al., 2008, *A&A*, 482, 699
- Cébron D., Moutou C., Le Bars M., Le Gal P., Farès R., 2011, in *European Physical Journal Web of Conferences*, Vol. 11, *European Physical Journal Web of Conferences*, p. 3003
- Cincotta P. M., Giordano C. M., Simó C., 2003, *Physica D Nonlinear Phenomena*, 182, 151
- Claret A., 2004, *A&A*, 428, 1001
- Collier Cameron A. et al., 2007, *MNRAS*, 380, 1230
- D’Angelo G., Lubow S. H., Bate M. R., 2006, *ApJ*, 652, 1698
- Dawson R. I., 2014, *ApJL*, 790, L31
- de Bruijne J. H. J., 2012, *Ap&SS*, 341, 31
- Deck K. M., Holman M. J., Agol E., Carter J. A., Lissauer J. J., Ragozzine D., Winn J. N., 2012, *ApJL*, 755, L21
- Delrez L. et al., 2014, *A&A*, 563, A143
- DENIS Consortium, 2005, *VizieR Online Data Catalog*, 2263, 0
- Doyle A. P., Davies G. R., Smalley B., Chaplin W. J., Elsworth Y., 2014, *MNRAS*, 444, 3592
- Doyle A. P. et al., 2013, *MNRAS*, 428, 3164
- Droege T. F., Richmond M. W., Sallman M. P., Creager R. P., 2006, *PASP*, 118, 1666
- Duffell P. C., Haiman Z., MacFadyen A. I., D’Orazio D. J., Farris B. D., 2014, *ApJL*, 792, L10
- Dupuy T. J., Kratter K. M., Kraus A. L., Isaacson H., Mann A. W., Ireland M. J., Howard A. W., Huber D., 2016, *ApJ*, 817, 80
- Dürmann C., Kley W., 2015, *A&A*, 574, A52
- Dvorak R., 1986, *A&A*, 167, 379
- Eastman J., Siverd R., Gaudi B. S., 2010, *PASP*, 122, 935
- Feroz F., Balan S. T., Hobson M. P., 2011, *MNRAS*, 416, L104
- Ford E. B., 2006, *ApJ*, 642, 505
- Fung J., Shi J.-M., Chiang E., 2014, *ApJ*, 782, 88
- Gaudi B. S., Winn J. N., 2007, *ApJ*, 655, 550
- Gillon M. et al., 2013, *A&A*, 552, A82
- Gillon M., Jehin E., Magain P., Chantry V., Hutsemékers D., Manfroid J., Queloz D., Udry S., 2011, in *European Physical Journal Web of Conferences*, Vol. 11, *European Physical Journal Web of Conferences*, p. 6002
- Gillon M. et al., 2012, *A&A*, 542, A4
- Giménez A., 2006, *ApJ*, 650, 408
- Goldreich P., Sari R., 2003, *ApJ*, 585, 1024
- Gray D. F., 2008, *The Observation and Analysis of Stellar Photospheres*, Gray, D. F., ed.
- Grether D., Lineweaver C. H., 2006, *ApJ*, 640, 1051
- Guillochon J., Ramirez-Ruiz E., Lin D., 2011, *ApJ*, 732, 74
- Hatzes A. P., Wuchterl G., 2005, *Nature*, 436, 182
- Hébrard G. et al., 2008, *A&A*, 488, 763
- Helled R. et al., 2014, *Protostars and Planets VI*, 643
- Hilditch R. W., 2001, *An Introduction to Close Binary Stars*, Hilditch, R. W., ed.
- Hinse T. C., Christou A. A., Alvarellos J. L. A., Goździewski K., 2010, *MNRAS*, 404, 837
- Holman M. J., Wiegert P. A., 1999, *AJ*, 117, 621
- Holman M. J. et al., 2006, *ApJ*, 652, 1715
- Huang C., Wu Y., Triaud A. H. M. J., 2016, *ApJ*, 825, 98
- Jehin E. et al., 2011, *The Messenger*, 145, 2
- Knutson H. A. et al., 2014, *ApJ*, 785, 126
- Kopal Z., 1942, *Proceedings of the National Academy of Science*, 28, 133
- Lai D., 2014, *MNRAS*, 440, 3532
- Lai D., Foucart F., Lin D. N. C., 2011, *MNRAS*, 412, 2790
- Lambrechts M., Johansen A., Morbidelli A., 2014, *A&A*, 572, A35
- Lang D., Hogg D. W., Mierle K., Blanton M., Roweis S., 2010, *AJ*, 139, 1782
- Lee E. J., Chiang E., 2015, *ApJ*, 811, 41
- Lendl M. et al., 2012, *A&A*, 544, A72
- , 2014, *A&A*, 568, A81

- Lin D. N. C., Bodenheimer P., Richardson D. C., 1996, *Nature*, 380, 606
- López-Morales M. et al., 2014, *ApJL*, 792, L31
- Lovis C. et al., 2006, *Nature*, 441, 305
- Madhusudhan N., Crouzet N., McCullough P. R., Deming D., Hedges C., 2014, *ApJL*, 791, L9
- Mandel K., Agol E., 2002, *ApJL*, 580, L171
- Mardling R. A., 2007, *MNRAS*, 382, 1768
- Marigo P., Girardi L., Bressan A., Groenewegen M. A. T., Silva L., Granato G. L., 2008, *A&A*, 482, 883
- Marmier M. et al., 2013, *A&A*, 551, A90
- Mayor M., Queloz D., 1995, *Nature*, 378, 355
- Naoz S., Farr W. M., Lithwick Y., Rasio F. A., Teyssandier J., 2011, *Nature*, 473, 187
- Neveu M., Sahlmann J., Queloz D., Ségransan D., 2012, in *Orbital Couples: Pas de Deux in the Solar System and the Milky Way*, Arenou F., Hestroffer D., eds., pp. 81–85
- Neveu-VanMalle M. et al., 2016, *A&A*, 586, A93
- Ortiz M. et al., 2016, *ArXiv e-prints*
- Perryman M., Hartman J., Bakos G. Á., Lindegren L., 2014, *ApJ*, 797, 14
- Perryman M. A. C. et al., 2001, *A&A*, 369, 339
- Petrovich C., 2015a, *ApJ*, 799, 27
- , 2015b, *ApJ*, 808, 120
- Pollacco D. L. et al., 2006, *PASP*, 118, 1407
- Pollack J. B., Hubickyj O., Bodenheimer P., Lissauer J. J., Podolak M., Greenzweig Y., 1996, *Icarus*, 124, 62
- Queloz D., Eggenberger A., Mayor M., Perrier C., Beuzit J. L., Naef D., Sivan J. P., Udry S., 2000, *A&A*, 359, L13
- Ragozzine D., Wolf A. S., 2009, *ApJ*, 698, 1778
- Ramm D. J., 2015, *MNRAS*, 449, 4428
- Rasio F. A., Ford E. B., 1996, *Science*, 274, 954
- Rein H., Spiegel D. S., 2015, *MNRAS*, 446, 1424
- Rein H., Tamayo D., 2015, *MNRAS*, 452, 376
- Rogers T. M., Lin D. N. C., McElwaine J. N., Lau H. H. B., 2013, *ApJ*, 772, 21
- Rosotti G. P., Booth R. A., Clarke C. J., Teyssandier J., Facchini S., Mustill A. J., 2016a, *ArXiv e-prints*
- Rosotti G. P., Juhasz A., Booth R. A., Clarke C. J., 2016b, *MNRAS*, 459, 2790
- Sahlmann J. et al., 2011, *A&A*, 525, A95
- Sahlmann J., Triaud A. H. M. J., Martin D. V., 2015, *MNRAS*, 447, 287
- Santerne A. et al., 2014, *A&A*, 571, A37
- , 2016, *A&A*, 587, A64
- Schlaufman K. C., 2010, *ApJ*, 719, 602
- Schneider J., Dedieu C., Le Sidaner P., Savalle R., Zolotukhin I., 2011, *A&A*, 532, A79
- Schwarz G., 1978, *Annals of Statistics*, 6, 461
- Seager S., Deming D., 2010, *ARA&A*, 48, 631
- Sestito P., Randich S., 2005, *A&A*, 442, 615
- Skrutskie M. F. et al., 2006, *AJ*, 131, 1163
- Southworth J. et al., 2009, *MNRAS*, 396, 1023
- Sozzetti A., Giacobbe P., Lattanzi M. G., Micela G., Morbidelli R., Tinetti G., 2014, *MNRAS*, 437, 497
- Spalding C., Batygin K., 2015, *ArXiv e-prints*
- Sterne T. E., 1939, *MNRAS*, 99, 451
- Stetson P. B., 1987, *PASP*, 99, 191
- Sutherland A. P., Fabrycky D. C., 2016, *ApJ*, 818, 6
- Teyssandier J., Ogilvie G. I., 2016, *MNRAS*, 458, 3221
- Thies I., Kroupa P., Goodwin S. P., Stamatellos D., Whitworth A. P., 2011, *MNRAS*, 417, 1817
- Torres G., Andersen J., Giménez A., 2010, *A&ApR*, 18, 67
- Tregloan-Reed J., Southworth J., 2013, *MNRAS*, 431, 966
- Triaud A. H. M. J., 2011, *A&A*, 534, L6
- Triaud A. H. M. J. et al., 2010, *A&A*, 524, A25
- , 2015, *MNRAS*, 450, 2279
- , 2009, *A&A*, 506, 377
- , 2011, *A&A*, 531, A24
- Ward W. R., 1997, *Icarus*, 126, 261
- Winn J. N., Fabrycky D. C., 2015, *ARA&A*, 53, 409
- Winn J. N., Johnson J. A., Albrecht S., Howard A. W., Marcy G. W., Crossfield I. J., Holman M. J., 2009, *ApJL*, 703, L99
- Wright J. T. et al., 2011, *PASP*, 123, 412
- Wu Y., Murray N. W., Ramsahai J. M., 2007, *ApJ*, 670, 820
- Zacharias N., Monet D. G., Levine S. E., Urban S. E., Gaume R., Wycoff G. L., 2004, in *Bulletin of the American Astronomical Society*, Vol. 36, American Astronomical Society Meeting Abstracts, p. 1418

APPENDIX A: JOURNAL OF OBSERVATIONS

Table A1: Radial velocities of WASP-53 obtained with CORALIE before its recent upgrade. BJD is the barycentric Julian date – 2 450 000 days. V_{rad} is the radial velocity obtained by fitting a cross-correlation function with a Gaussian, σ_{RV} is the error on V_{rad} . FWHM is the full width at half maximum of the cross-correlation function, and contrast is the amplitude.

BJD (days)	V_{rad} (km s ⁻¹)	σ_{RV} (km s ⁻¹)	FWHM (km s ⁻¹)	contrast (%)	slope bisector span (km s ⁻¹)	exposure (sec)
55535.622498	-4.38964	0.01414	7.76355	37.811	0.00572	1800.679
55563.633734	-4.75981	0.01675	7.83813	38.764	-0.01915	1800.736
55565.620787	-4.10113	0.02222	7.85708	29.332	0.06569	1800.743
55583.571236	-4.53580	0.01833	7.76400	37.735	-0.01908	1800.754
55586.577359	-4.45769	0.01936	7.88629	36.602	0.03945	1800.755
55588.564415	-3.81514	0.02958	7.88939	36.377	0.10109	1800.756
55591.537016	-3.85825	0.01594	7.85784	37.219	0.01104	1800.759
55593.534932	-4.43614	0.02059	7.88560	36.521	0.01531	1800.758
55595.533798	-3.86707	0.02407	7.86921	36.778	0.01591	1800.859
55596.534633	-4.37790	0.01454	7.89625	37.250	0.02008	1800.739
55599.531272	-4.19644	0.02246	7.82083	35.628	0.04899	1800.775
55600.531357	-4.32590	0.02605	7.81524	34.950	0.02073	1800.736
55613.530286	-4.35247	0.03126	7.75947	35.915	0.02255	1800.830
55614.520174	-3.80772	0.03751	7.98353	12.241	0.08784	1800.768
55619.515487	-4.11077	0.03829	7.86610	12.606	0.07253	1800.726
55624.511532	-3.81662	0.04668	7.99027	31.484	0.16010	1800.767
55769.931969	-3.69384	0.03211	7.83406	40.671	-0.01480	1800.816
55770.811670	-3.50787	0.01869	7.84814	40.222	0.05379	1800.797
55772.921899	-3.88919	0.02320	7.76734	20.208	0.03801	1800.748
55777.849432	-3.68608	0.01545	7.81802	39.166	-0.01838	1800.821
55782.883847	-3.89564	0.01539	7.75827	40.337	0.05484	1800.740
55802.854702	-3.81609	0.01659	7.79265	40.844	0.00480	1800.739
55806.876427	-3.49432	0.01352	7.77050	40.390	-0.00408	1800.777
55809.812708	-3.62453	0.01453	7.85935	40.282	-0.03700	1800.739
55810.864649	-3.61455	0.01691	7.82177	40.031	0.00585	1800.798
55811.834443	-4.11173	0.01961	7.82148	39.929	-0.00983	1800.777
55825.779642	-3.93644	0.01342	7.83048	39.001	-0.03320	1800.718
55826.823506	-3.49648	0.02008	7.81726	39.820	-0.10400	1800.818
55834.845196	-4.07174	0.01455	7.82559	40.420	0.02738	1800.758
55852.655157	-3.71694	0.01847	7.89498	39.010	-0.02472	1800.759
55869.776795	-3.46744	0.01511	7.84842	39.370	-0.03676	1800.736
55887.725010	-4.01495	0.01502	7.76766	39.004	0.02644	1800.754
55889.585568	-3.46497	0.01504	7.78976	38.829	-0.01253	1800.755
55910.593618	-3.84547	0.01446	7.80091	39.026	-0.05197	1800.778
55952.575538	-3.44630	0.01294	7.90378	38.024	0.02529	1800.688
55974.534361	-4.02707	0.02632	7.83726	38.734	-0.02393	1800.748
56101.929818	-3.49841	0.02543	7.87117	40.333	-0.02903	1800.799
56108.902853	-3.68569	0.03173	7.87649	39.586	0.02577	1800.940
56130.929240	-3.54201	0.02272	7.82397	39.617	-0.10018	1800.817
56158.920126	-3.87751	0.02491	7.83489	39.943	-0.04714	1800.781
56165.794126	-3.99424	0.02180	7.84562	35.852	-0.00917	1800.759
56166.840915	-3.81564	0.01755	7.86863	39.564	-0.03721	1800.777
56182.742965	-4.11729	0.01762	7.83280	38.786	0.04594	1800.798
56184.735109	-3.50543	0.01419	7.81771	39.385	-0.00971	1800.758
56186.764241	-3.81243	0.01735	7.89344	39.090	0.05377	1800.778
56190.675191	-3.46799	0.02295	7.92760	37.779	0.04893	1800.820
56196.864653	-3.71479	0.01309	7.83567	38.860	-0.02100	2700.667
56235.613045	-4.09012	0.02545	7.83788	37.690	0.01474	1800.777
56245.697375	-4.06430	0.01518	7.90888	37.534	0.00491	1800.756
56264.722841	-3.84938	0.01631	7.88340	39.189	0.03949	1800.749
56309.616625	-3.61756	0.01619	7.91453	40.096	-0.03900	1800.739
56335.551640	-3.93777	0.02599	8.01659	39.469	0.01497	1800.758
56460.921265	-4.08678	0.01861	7.87168	43.357	-0.00289	1800.756
56490.864375	-4.05183	0.02101	7.86144	40.429	-0.05535	1800.755

Table continues next page...

JDB (days)	V_{rad} (km s^{-1})	σ_{RV} (km s^{-1})	FWHM (km s^{-1})	contrast (%)	slope bisector span (km s^{-1})	exposure (sec)
56505.803479	-3.53226	0.01677	7.88179	41.428	0.04581	1800.799
56516.868634	-4.11013	0.02259	7.86987	41.506	-0.04888	1800.857
56538.754792	-3.46848	0.02937	7.87498	40.897	0.01746	1800.779
56543.888666	-3.98696	0.01538	7.87143	39.824	0.02301	1800.763
56544.693786	-3.50813	0.03240	7.85548	41.040	0.06695	1800.802
56545.715662	-3.63146	0.01620	7.94485	37.812	-0.00368	1800.819
56562.781196	-3.94366	0.01417	7.82567	40.715	-0.00693	1800.786
56563.802018	-3.97705	0.01494	7.91152	40.932	0.00453	1800.836
56565.713332	-3.68586	0.01541	7.84101	40.339	0.00271	1800.777
56567.702293	-3.59801	0.02820	7.86619	41.893	0.03071	1800.775
56591.740189	-3.50574	0.01941	7.79994	39.462	0.00814	1800.719
56603.739663	-3.82508	0.01907	7.84847	40.983	0.01256	1800.779
56644.683453	-3.51463	0.01493	7.76010	38.600	-0.01970	1800.778
56682.557464	-4.10162	0.01957	7.85501	40.062	-0.00216	1800.770
56817.930262	-4.05370	0.02181	7.86074	41.914	0.01356	1602.786
56877.826276	-4.07700	0.01910	7.80224	38.824	0.01261	1800.058
56878.777852	-3.63053	0.03452	7.88373	34.977	0.04216	1800.685
56920.870295	-4.12036	0.01832	7.83603	39.391	-0.03675	1800.677
56961.797598	-3.54257	0.01781	7.78155	38.574	0.05712	1800.601

Table A2: Radial velocities of WASP-53 obtained with CORALIE after its recent upgrade. BJD is the barycentric Julian date $- 2\,450\,000$ days. V_{rad} is the radial velocity obtained by fitting a cross-correlation function with a Gaussian, σ_{RV} is the error on V_{rad} . FWHM is the full width at half maximum of the cross-correlation function, and contrast is the amplitude.

BJD (days)	V_{rad} (km s^{-1})	σ_{RV} (km s^{-1})	FWHM (km s^{-1})	contrast (%)	slope bisector span (km s^{-1})	exposure (sec)
56989.740666	-3.92092	0.02509	7.82426	42.096	-0.11250	1800.683
57001.640882	-3.53647	0.02300	7.73609	42.361	0.00145	1800.780
57003.640065	-4.11709	0.01937	7.71262	41.800	-0.01624	1800.075
57004.682396	-3.59763	0.02263	7.74968	41.276	-0.00541	1800.932
57012.592977	-3.75798	0.02566	7.80047	42.030	-0.03335	1800.233
57027.631091	-3.72146	0.03574	7.68990	38.087	0.04302	1800.770
57063.528866	-4.02456	0.05181	7.77355	41.187	-0.02410	1800.102
57065.534295	-3.74442	0.03302	7.76903	41.060	-0.00757	1800.943
57192.938473	-3.84251	0.03767	7.74347	45.120	0.01185	1800.861
57205.925822	-3.96730	0.04649	7.82306	42.941	0.03207	1800.925
57261.823294	-4.14072	0.04184	7.70847	43.479	0.00495	1800.924
57341.740033	-3.88956	0.05660	7.82722	43.813	-0.08024	1800.895
57362.678177	-3.49435	0.01850	7.75263	43.012	-0.00904	2700.715
57367.607494	-4.16776	0.02672	7.72596	43.081	0.00961	2700.804
57381.547386	-3.92186	0.02486	7.66936	41.940	-0.00042	2700.686
57389.610441	-3.61683	0.02988	7.76154	43.413	-0.02558	1800.083
57413.581920	-4.09479	0.03288	7.77853	41.771	0.04996	2700.626
57587.836041	-3.52915	0.02814	7.79372	41.294	-0.06745	1800.382
57616.796911	-3.78390	0.02024	7.67173	42.253	-0.03829	1800.431
57681.574518	-4.02549	0.03158	7.69350	43.049	0.03337	1800.382
57689.706629	-3.71986	0.02108	7.72289	42.465	0.02337	1800.354
57691.675531	-4.13251	0.01765	7.72530	42.658	-0.01465	1800.394
57711.743027	-4.18272	0.03598	7.68311	42.736	-0.03452	1800.352
57713.676572	-3.56151	0.02072	7.80813	42.301	-0.01114	1800.353
57713.698411	-3.54916	0.02373	7.77659	42.830	-0.04693	1800.372

Table A3: Radial velocities of WASP-53 obtained with HARPS. BJD is the barycentric Julian date – 2 450 000 days. V_{rad} is the radial velocity obtained by fitting a cross-correlation function with a Gaussian, σ_{RV} is the error on V_{rad} . FWHM is the full width at half maximum of the cross-correlation function, and contrast is the amplitude.

BJD (days)	V_{rad} (km s ⁻¹)	σ_{RV} (km s ⁻¹)	FWHM (km s ⁻¹)	contrast (%)	slope bisector span (km s ⁻¹)	exposure (sec)
55802.804248	-3.87536	0.01428	6.35185	48.819	0.01421	900.000
55802.902737	-3.77124	0.00615	6.44231	49.068	0.01648	900.000
55803.735877	-3.46797	0.00592	6.43227	49.138	0.02630	900.000
55803.876858	-3.49415	0.01413	6.44454	48.445	0.03957	900.000
55825.652716	-4.00995	0.00918	6.43519	50.675	-0.00062	900.006
55825.842017	-3.90801	0.00695	6.40550	50.365	0.03042	900.006
55826.656742	-3.47586	0.00682	6.42903	50.419	0.03065	900.006
55826.837326	-3.44345	0.00407	6.45292	49.300	0.02401	900.006
55827.646391	-3.74232	0.01085	6.42916	48.557	0.03541	600.000
55827.656368	-3.74253	0.00678	6.46451	48.782	0.01240	900.006
55827.669238	-3.75174	0.00631	6.49718	48.731	0.01620	900.006
55827.680986	-3.73814	0.00634	6.46326	48.738	0.05819	900.001
55827.692515	-3.74724	0.00573	6.44915	49.065	0.00441	900.006
55827.703846	-3.77343	0.00561	6.42803	49.040	0.01460	900.006
55827.715374	-3.78034	0.00546	6.47191	48.934	0.01938	900.006
55827.726810	-3.78879	0.00536	6.45148	49.091	0.00973	900.001
55827.738546	-3.79623	0.00512	6.43309	49.178	0.00681	900.006
55827.749681	-3.81542	0.00512	6.43640	49.235	0.01215	900.006
55827.761637	-3.80869	0.00518	6.44554	49.108	0.02622	900.006
55827.773177	-3.80569	0.00438	6.43072	49.362	0.02610	900.006
55827.784612	-3.81191	0.00451	6.43123	49.319	0.01551	900.006
55827.796036	-3.82316	0.00414	6.44297	49.391	0.03097	900.006
55827.807576	-3.83545	0.00448	6.44773	49.167	0.01898	900.006
55827.819324	-3.84303	0.00454	6.43978	49.196	0.03451	900.006
55827.830760	-3.84995	0.00553	6.47049	48.899	0.00391	900.006
55827.842091	-3.84996	0.00523	6.47341	48.922	0.00081	900.006
55828.639175	-4.09963	0.00613	6.47747	48.749	0.01814	900.006
55828.880860	-4.04309	0.00432	6.47502	49.127	0.01328	900.006
55831.640517	-4.07244	0.00490	6.49495	48.903	0.00429	900.006
55831.862305	-4.09707	0.00367	6.44317	49.351	0.03159	900.006
56108.917970	-3.67055	0.01289	6.48511	48.048	0.01989	900.000
56109.931976	-4.08058	0.00352	6.42686	49.455	0.01035	1800.000
56158.807248	-3.82192	0.00781	6.45609	48.928	0.02814	600.000
56159.819284	-4.04984	0.01179	6.43642	49.040	0.01204	600.006
56190.816064	-3.45497	0.00746	6.40310	49.253	0.02240	899.999
56191.702180	-3.70159	0.00717	6.40858	49.055	0.05467	799.999
56191.713245	-3.70009	0.00584	6.40354	49.321	0.02801	900.000
56191.724577	-3.69652	0.00596	6.39529	49.155	0.05629	900.000
56191.736348	-3.72787	0.00617	6.41546	49.184	0.01366	899.999
56191.747992	-3.72226	0.00600	6.41604	49.269	0.01401	900.000
56191.759624	-3.72504	0.00565	6.37832	49.470	0.04169	900.000
56191.771060	-3.72870	0.00555	6.39147	49.478	0.02959	900.000
56191.782391	-3.74305	0.00534	6.39205	49.326	0.01126	900.000
56191.794012	-3.74230	0.00596	6.39070	49.423	0.03308	900.000
56191.805748	-3.74590	0.00535	6.39200	49.398	0.01416	900.006
56191.817172	-3.76612	0.00464	6.40073	49.412	0.00858	899.999
56191.828724	-3.77051	0.00455	6.39737	49.586	0.01365	899.999
56191.840043	-3.79008	0.00529	6.40980	49.416	0.01943	900.000
56191.851583	-3.78008	0.00543	6.41797	49.150	0.03092	900.006
56191.863100	-3.78198	0.00526	6.40679	49.445	0.02901	900.006
56191.874628	-3.79791	0.00667	6.40276	49.074	0.02995	900.006
56191.886168	-3.80101	0.00761	6.47274	48.383	0.02179	900.006
56191.897592	-3.80062	0.00746	6.45821	48.542	0.03297	900.006
56191.909027	-3.82351	0.00717	6.48428	47.642	-0.00093	900.000

Table continues next page...

JDB (days)	V_{rad} (km s ⁻¹)	σ_{RV} (km s ⁻¹)	FWHM (km s ⁻¹)	contrast (%)	slope	bisector span (km s ⁻¹)	exposure (sec)
56192.821879	-4.07292	0.00787	6.41754	48.966		0.05738	600.006
56193.794605	-3.56742	0.01278	6.43435	48.521		-0.07894	599.999
56215.823377	-4.10629	0.00762	6.50823	48.183		0.00481	900.000
56221.537217	-3.74752	0.01691	6.51008	49.285		0.02560	899.999
56239.592460	-3.87591	0.00851	6.45703	48.675		-0.00723	600.004
56256.602476	-3.60375	0.01122	6.44653	47.974		0.02296	600.000
56257.580498	-3.53847	0.00792	6.44921	48.513		0.02276	600.008
56264.522496	-3.70152	0.00630	6.42133	48.725		0.02209	700.000
56264.535284	-3.70567	0.00475	6.44658	49.066		0.03476	900.000
56264.547494	-3.71370	0.00443	6.45767	49.036		0.00891	900.001
56264.559264	-3.72208	0.00418	6.43897	49.154		0.01169	900.001
56264.571220	-3.72100	0.00415	6.45931	49.191		0.02381	900.000
56264.583638	-3.72408	0.00410	6.43960	49.306		0.02411	900.001
56264.595350	-3.73021	0.00391	6.43981	49.248		0.00984	900.001
56264.607201	-3.73698	0.00406	6.45517	49.099		0.04027	900.001
56264.619145	-3.74812	0.00392	6.43708	49.233		0.01867	900.000
56264.630926	-3.76424	0.00387	6.43620	49.161		0.01727	900.001
56264.643541	-3.77312	0.00419	6.45208	49.142		0.02687	900.000
56264.655415	-3.78187	0.00454	6.44031	48.969		-0.00318	900.000
56264.667243	-3.77665	0.00507	6.47638	48.785		0.02202	900.001
56264.679106	-3.78417	0.00526	6.45092	48.850		0.02116	900.000
56264.700945	-3.80013	0.00563	6.44897	48.770		-0.00597	900.000
56307.533598	-3.69537	0.00686	6.45089	48.804		0.01119	600.001
56323.548244	-3.45869	0.00931	6.50816	48.367		0.03162	600.001
56460.933662	-4.06790	0.01142	6.50197	48.107		0.02895	600.000
56567.891937	-3.50754	0.00974	6.50537	48.057		0.03808	900.000
56608.727539	-3.69785	0.01233	6.50649	49.948		-0.01752	900.001
56927.722485	-4.07286	0.00838	6.44451	50.116		0.04495	900.001
56928.789883	-3.51368	0.00559	6.43032	49.834		0.02100	900.001

Table A4: Radial velocities of WASP-81 obtained with CORALIE before its recent upgrade. BJD is the barycentric Julian date - 2 450 000 days. V_{rad} is the radial velocity obtained by fitting a cross-correlation function with a Gaussian, σ_{RV} is the error on V_{rad} . FWHM is the full width at half maximum of the cross-correlation function, and contrast is the amplitude.

BJD (days)	V_{rad} (km s ⁻¹)	σ_{RV} (km s ⁻¹)	FWHM (km s ⁻¹)	contrast (%)	slope	bisector span (km s ⁻¹)	exposure (sec)
55833.506244	-60.15011	0.02609	7.87708	28.619		-0.02494	1800.760
55834.511338	-60.31782	0.01861	8.06275	28.959		0.00051	1800.778
55835.513064	-60.23827	0.02606	7.95214	29.089		-0.10707	1800.742
55851.553175	-60.35013	0.02264	7.95814	26.734		-0.00195	1800.720
55852.509304	-60.17890	0.02674	7.99858	27.682		0.01749	1800.738
55856.541346	-60.33501	0.02613	7.94386	25.704		0.08807	1800.760
55859.509870	-60.34664	0.02357	7.88504	28.508		-0.00745	1800.780
55862.507592	-60.34739	0.02726	8.04740	28.210		0.02566	1800.736
56050.916807	-60.48137	0.02097	8.07575	29.178		-0.02474	1800.735
56067.826597	-60.58673	0.02138	8.03943	30.584		0.00355	1800.755
56068.860596	-60.68491	0.02516	8.05512	30.442		0.03245	1800.776
56069.893252	-60.54821	0.03319	8.04313	30.912		-0.07498	1800.735
56075.788615	-60.51078	0.02761	8.02011	30.192		-0.01121	1800.778
56076.818326	-60.73022	0.03529	8.07559	30.163		-0.04915	1800.798
56101.786777	-60.65253	0.02870	7.97893	30.248		-0.05570	1800.841
56103.782366	-60.71255	0.01969	8.04937	30.321		0.05327	1800.796
56108.832891	-60.72716	0.03353	8.05096	30.385		-0.06728	1800.796
56133.765892	-60.75905	0.02643	8.07510	30.056		-0.04689	1800.777
56135.751516	-60.64218	0.03190	8.09815	28.651		-0.14222	1800.753
56147.744152	-60.73914	0.04144	7.95476	26.863		-0.04738	2700.746
56151.718366	-60.56578	0.02640	7.99750	29.524		0.08671	2700.607
56154.664701	-60.64301	0.05536	8.11592	29.581		-0.05746	1800.799

Table continues next page...

JDB (days)	V_{rad} (km s ⁻¹)	σ_{RV} (km s ⁻¹)	FWHM (km s ⁻¹)	contrast (%)	slope bisector span (km s ⁻¹)	exposure (sec)
56158.595576	-60.75601	0.02555	7.92280	30.002	-0.02869	1800.841
56181.617460	-60.64235	0.01367	7.97978	29.506	0.01627	2700.606
56182.616959	-60.80774	0.01615	7.95422	29.259	0.01257	2700.707
56204.525708	-60.82325	0.02655	8.06633	27.984	-0.01402	2700.603
56230.518367	-60.64910	0.02851	7.95769	22.694	-0.00547	2700.696
56431.902050	-60.84674	0.02090	7.98365	30.384	-0.00998	2700.679
56455.806063	-60.72687	0.02870	7.95465	29.802	-0.02273	1800.797
56487.786778	-60.74249	0.02033	7.98515	30.749	0.00328	2700.713
56509.710623	-60.66513	0.01397	7.95360	30.834	-0.02276	2700.732
56511.692477	-60.85952	0.02225	7.94794	30.979	0.01657	1800.741
56518.621811	-60.71971	0.01770	7.97615	30.608	0.00907	1620.506
56531.555446	-60.63273	0.03202	7.97035	29.748	0.00804	2700.637
56547.652096	-60.58724	0.01827	8.03302	30.090	0.02345	2700.599
56548.506904	-60.61018	0.01534	7.99134	28.749	-0.03196	2700.680
56556.531108	-60.54362	0.05433	8.01616	29.137	-0.01045	2700.631
56560.494763	-60.71382	0.03762	7.96320	29.254	0.01284	1800.774
56565.533770	-60.70908	0.01949	7.86719	29.094	-0.02711	2700.712
56573.536534	-60.65052	0.01500	7.97570	29.996	-0.00324	2700.713
56585.548076	-60.46305	0.01694	7.98314	29.017	0.05210	2700.649
56595.517658	-60.51555	0.01739	7.94433	29.102	0.00994	2700.571
56602.513782	-60.25658	0.02280	8.11640	27.697	0.02679	2700.797
56610.522915	-60.19533	0.02343	7.99369	28.294	0.07335	2700.613
56764.896812	-58.50304	0.01351	8.03570	30.083	0.00910	2700.766
56776.887472	-58.68466	0.02343	7.97764	30.796	0.02733	2700.763
56804.815200	-58.96099	0.02049	7.95361	30.061	-0.00476	2700.910
56811.785740	-58.86942	0.01887	8.04819	30.119	0.03930	2700.909
56835.751223	-59.01187	0.03321	8.10950	28.842	-0.03052	2700.800
56856.750436	-59.28657	0.01680	8.01407	29.501	-0.03712	2700.187
56886.668064	-59.46175	0.01926	7.92853	30.839	-0.03399	2700.767
56920.621957	-59.54393	0.02171	8.03739	27.815	-0.01603	2700.428
56954.527818	-59.78127	0.02459	7.99078	24.160	0.00379	2699.955

Table A5: Radial velocities of WASP-81 obtained with CORALIE before its recent upgrade. BJD is the barycentric Julian date - 2 450 000 days. V_{rad} is the radial velocity obtained by fitting a cross-correlation function with a Gaussian, σ_{RV} is the error on V_{rad} . FWHM is the full width at half maximum of the cross-correlation function, and contrast is the amplitude.

BJD (days)	V_{rad} (km s ⁻¹)	σ_{RV} (km s ⁻¹)	FWHM (km s ⁻¹)	contrast (%)	slope bisector span (km s ⁻¹)	exposure (sec)
57186.791639	-60.24486	0.03042	7.95261	34.569	0.01499	2700.846
57194.736148	-60.23109	0.04093	7.89406	34.000	0.06709	2700.943
57211.722549	-60.44937	0.06100	7.91874	33.627	-0.06934	2700.764
57256.542816	-60.39378	0.04425	7.97087	32.551	-0.07702	2700.014
57271.550777	-60.56686	0.04207	7.93436	32.440	-0.11635	2452.822
57294.561176	-60.47338	0.03198	7.90803	32.325	0.03218	2700.157
57324.515825	-60.41128	0.05112	7.96576	32.327	0.01866	2700.768
57584.816334	-60.83346	0.09427	8.04004	33.592	0.00022	600.528
57595.700710	-60.85481	0.05770	7.87866	32.934	-0.16166	1800.381
57650.537435	-60.75600	0.02171	7.81752	32.403	-0.05037	2700.072
57652.595356	-60.87248	0.01754	7.90775	32.227	-0.03345	2700.069
57661.566328	-60.75291	0.01948	7.98951	32.002	-0.09351	2700.037
57680.545006	-60.81445	0.04449	7.85147	31.815	0.02024	1800.422
57682.504365	-60.89638	0.02700	7.86095	32.269	-0.03440	1800.000

Table A6: Radial velocities of WASP-81 obtained with HARPS. BJD is the barycentric Julian date – 2 450 000 days. V_{rad} is the radial velocity obtained by fitting a cross-correlation function with a Gaussian, σ_{RV} is the error on V_{rad} . FWHM is the full width at half maximum of the cross-correlation function, and contrast is the amplitude. One datum, which was not used in the analysis, is highlighted with an asterisk.

BJD (days)	V_{rad} (km s ⁻¹)	σ_{RV} (km s ⁻¹)	FWHM (km s ⁻¹)	contrast (%)	slope bisector span (km s ⁻¹)	exposure (sec)
6403.902377	-60.75558	0.01422	6.77096	36.778	0.00282	600.000
6407.886489	-60.90138	0.01261	6.79512	36.264	0.02080	600.001
6411.902064*	-73.15969	0.09454	1.71111	2.286	789.3231	600.000
6438.878243	-60.76828	0.01674	6.81762	37.631	-0.00578	900.000
6454.847018	-60.87117	0.01534	6.72971	36.706	-0.03163	600.001
6457.848776	-60.77664	0.02008	6.77591	36.474	0.00183	600.001
6459.922794	-60.93969	0.01386	6.78047	36.319	-0.02629	600.001
6510.582235	-60.74526	0.01857	6.81107	36.977	0.06192	600.001
6510.591263	-60.70229	0.01341	6.82417	36.599	0.00540	600.001
6510.601795	-60.72294	0.00980	6.75473	36.746	-0.00742	900.002
6510.613242	-60.73820	0.00957	6.85763	36.762	-0.01984	900.001
6510.624769	-60.72645	0.00900	6.77831	36.900	-0.03973	900.000
6510.636309	-60.73310	0.00930	6.79062	36.931	-0.04372	900.001
6510.647628	-60.74584	0.00988	6.77485	36.935	0.00680	900.001
6510.659260	-60.74602	0.00985	6.78777	37.029	0.00791	900.001
6510.670810	-60.75529	0.01062	6.81317	37.005	0.01163	900.001
6510.682546	-60.75335	0.01157	6.77487	37.079	-0.04139	900.000
6510.693877	-60.74670	0.01072	6.78601	36.671	-0.02780	900.002
6510.705324	-60.74468	0.01284	6.76216	36.814	0.02584	900.001
6510.717072	-60.75111	0.01365	6.77729	36.867	0.01253	900.001
6510.728495	-60.75617	0.01286	6.80405	36.945	-0.03819	900.001
6510.740046	-60.78206	0.01203	6.75481	37.010	-0.00396	900.000
6510.751689	-60.77077	0.01090	6.79623	36.943	-0.00076	900.001
6510.763124	-60.75516	0.01073	6.76794	37.020	-0.01169	900.001
6510.774455	-60.75574	0.01039	6.79067	36.959	0.00137	900.001
6510.786527	-60.78525	0.01380	6.74017	36.801	-0.01100	900.000
6511.701655	-60.81984	0.01049	6.77291	36.841	-0.03984	900.001
6564.490867	-60.51083	0.01246	6.78860	36.623	-0.02331	600.001
6565.479782	-60.69072	0.01538	6.75616	35.156	-0.01447	600.000
6736.904747	-58.61384	0.01996	6.74955	37.023	-0.06442	900.001
6761.912737	-58.54571	0.01394	6.80035	37.818	-0.03933	900.001
6801.852737	-58.92484	0.03752	6.73650	39.960	0.02316	900.001
6927.561062	-59.65603	0.01215	6.81727	37.578	-0.01936	900.002

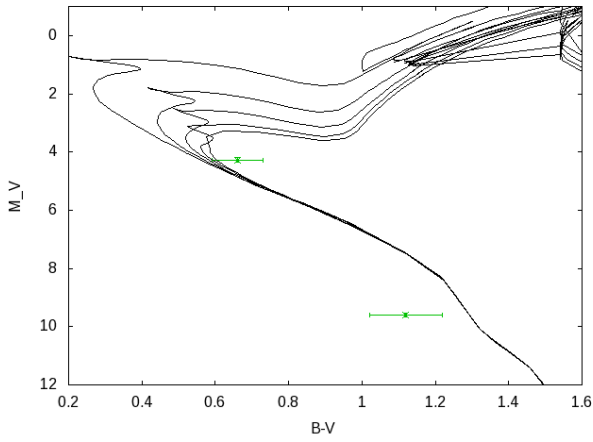


Figure B1. Hertzsprung–Russell diagram showing the relative positions of WASP-81A and WASP-81B assuming a similar distance. The pair is unlikely to be related. Models are from [Marigo et al. \(2008\)](#).

APPENDIX B: THE VISUAL COMPANION TO WASP-81

APPENDIX C: MODELS APPLIED TO THE PHOTOMETRIC DATA

This paper has been typeset from a \TeX / \LaTeX file prepared by the author.

System	Date	Instrument	Filter	T_{exp}	N_p	Baseline function	CF
WASP-53	2011-07-22	EulerCAM	Gunn r'	90s	110	$p(t^2 + xy)$	1.3
WASP-53	2011-09-03	EulerCAM	Gunn r'	120s	84	$p(t^2 + xy)$	1.8
WASP-53	2011-09-13	TRAPPIST	blue blocking	12s	744	$p(t^2) + o$	1.5
WASP-53	2011-09-13	EulerCAM	Gunn r'	80s	127	$p(t^2 + xy + \sin(P_3t + T_{0,3}))$	1.7
WASP-53	2011-09-23	EulerCAM	Gunn r'	180s	77	$p(t^2 + xy + \sin(P_4t + T_{0,4}))$	2.3
WASP-53	2011-10-26	EFOSC2	Gunn r'	150s	54	$p(t^2)$	1.0
WASP-53	2012-07-30	TRAPPIST	blue blocking	12s	603	$p(t^2)$	1.5
WASP-53	2012-11-03	TRAPPIST	$I + z'$	15s	464	$p(t^2)$	1.0
WASP-81	2011-09-26	TRAPPIST	$I + z'$	12s	287	$p(t^2) + o$	0.9
WASP-81	2012-05-20	TRAPPIST	$I + z'$	25s	372	$p(t^2) + o$	1.1
WASP-81	2012-05-31	TRAPPIST	$I + z'$	12s	812	$p(t^2) + o$	1.4
WASP-81	2012-06-19	TRAPPIST	<i>blueblocking</i>	8s	644	$p(t^2) + o$	1.5
WASP-81	2012-07-08	EulerCAM	Gunn r'	120s	116	$p(t^2)$	1.9
WASP-81	2012-07-19	TRAPPIST	$I + z'$	20s	501	$p(t^2) + o$	1.6
WASP-81	2012-09-24	EulerCAM	Gunn r'	120s	132	$p(t^2)$	1.4
WASP-81	2013-07-07	TRAPPIST	blue blocking	10s	917	$p(t^2) + o$	1.9
WASP-81	2013-08-06	EulerCAM	Gunn r'	80s	248	$p(t^2)$	1.4
WASP-81	2013-08-06	TRAPPIST	blue blocking	10s	1082	$p(t^2) + o$	1.3

Table C1. Photometric time-series used in this work. For each light curve this table shows the date of acquisition, the instrument and filter used, the exposure time T_{exp} , the number of data points, the baseline function selected for our global analysis (see Sec. 5), and the error correction factor CF used in our global analysis. For the baseline function, $p(\epsilon^N)$ denotes, respectively, a N -order polynomial function of time ($\epsilon = t$), x and y positions ($\epsilon = xy$); o denotes an offset at the time of a meridian flip of TRAPPIST (see Gillon et al. 2012). On two instances we also fit a sinusoidal baseline of the form $\sin(Pt + T_0)$ where P is the period, and T_0 is the phase.

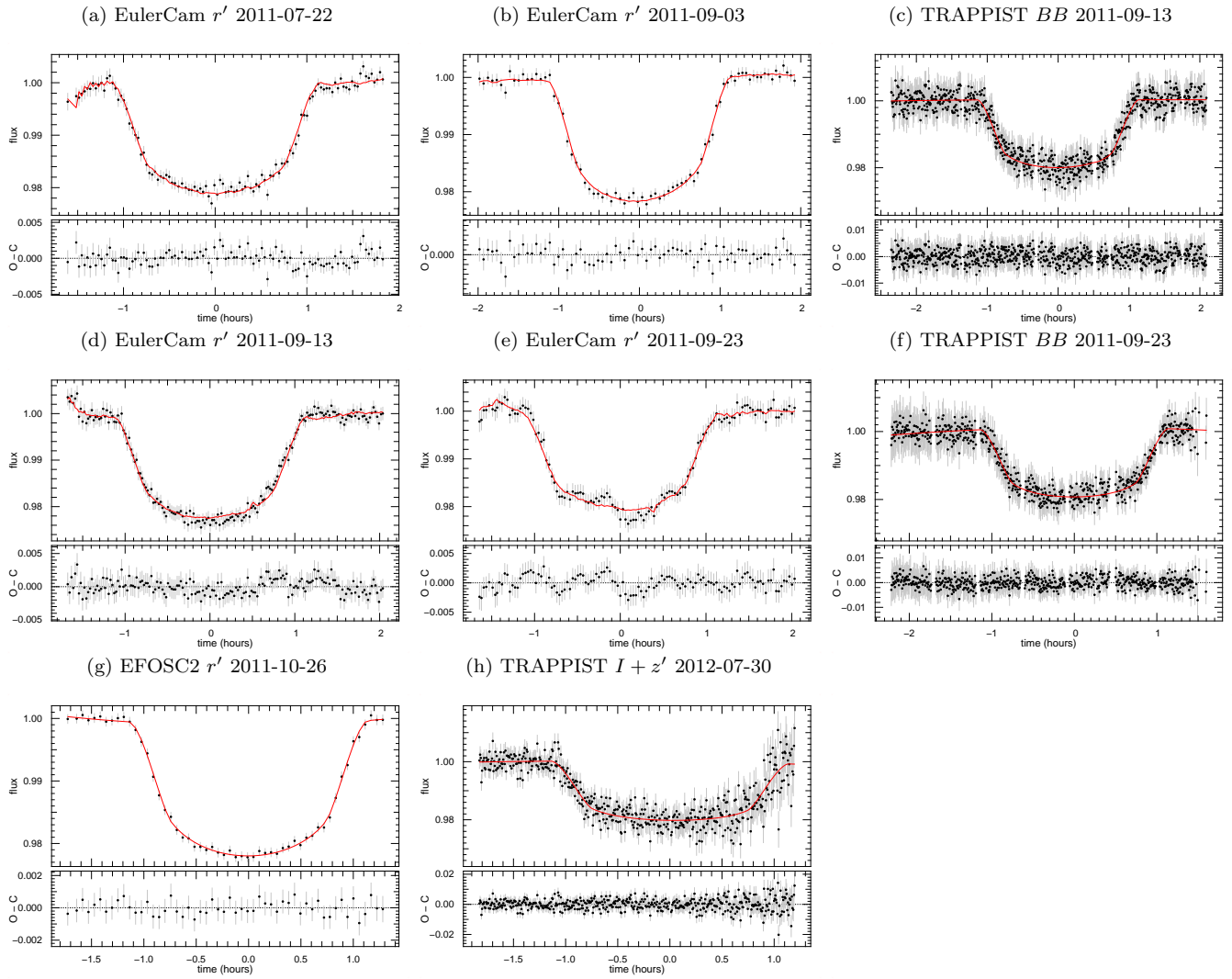


Figure C1. Flux as a function of time, centred around mid-transit time of WASP-53b. The red line shows the full model, including the detrending.

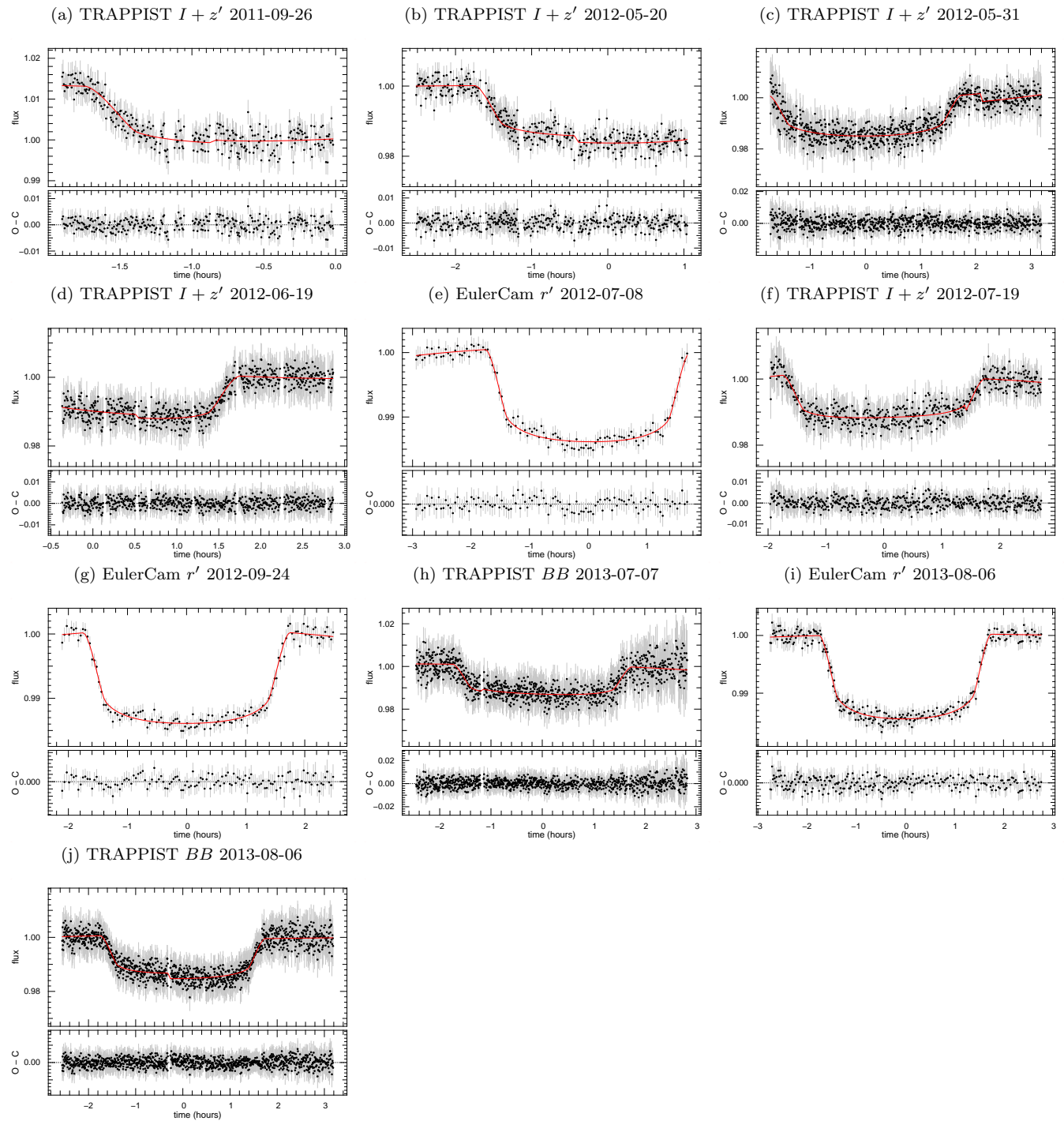


Figure C2. Flux as a function of time, centred around mid-transit time of WASP-81b. The red line shows the full model, including the detrending.